MECHANICAL ANALYSIS OF SPINAL IMPLANTS IN PATIENTS WITH ADOLESCENT IDIOPATHIC SCOLIOSIS

A DISSERTATION SUBMITTED TO
THE GRADUATE SCHOOL OF
ENGINEERING AND NATURAL SCIENCES
OF ISTANBUL MEDIPOL UNIVERSITY
IN PARTIAL FULFILLMENT OF THE REQUIREMENTS FOR
THE DEGREE OF
DOCTOR OF PHILOSOPHY
IN
BIOMEDICAL ENGINEERING AND BIOINFORMATICS

By

Saliha Zeyneb AKINCI

June, 2022

MECHANICAL ANALYSIS OF SPINAL IMPLANTS IN PATIENTS WITH ADOLESCENT IDIOPATHIC SCOLIOSIS

By Saliha Zeyneb AKINCI

24 June 2022

We certify that we have read this dissertation and that in our opinion it is fully adequate, in scope and in quality, as a dissertation for the degree of Doctor of Philosophy.

_____

Prof. Dr. Yunus Ziya ARSLAN (Advisor)

_____

Prof. Dr. Onur YAMAN

_____

Prof. Dr. Yasemin YÜKSEL DURMAZ

_____

Assoc. Prof. Dr. Mehmet Kemal ÖZDEMİR

_____

Assist. Prof. Dr. Hasan Kemal SÜRMEN

Approved by the Graduate School of Engineering and Natural Sciences:

_____

Prof. Dr. Yasemin YÜKSEL DURMAZ

Director of the Graduate School of Engineering and Natural Sciences

I hereby declare that all information in this document has been obtained and presented in accordance with the academic rules and ethical conduct. I also declare that, as required by these rules and conduct, I have fully cited and referenced all material and results that are not original to this work.

Signature :

Name, Surname: SALİHA ZEYNEB AKINCI

ACKNOWLEDGEMENT

I would like to express my sincere gratitude to my advisor Prof. Dr. Yunus Ziya Arslan for the continuous support also his patience during my Ph.D. research. Being a member of his biomechanics research group is a great opportunity for me to collaborate with other researchers. His encouragement and immense knowledge guided me to continue my studies.

Besides, I would also like to thank the other members of my thesis committee: Prof. Dr. Onur Yaman, and Assist. Prof. Dr. Hasan Kemal Sürmen for their encouragement and valuable comments. I am grateful to them for enlightening me to pursue this research.

My sincere thanks also go to Prof. Dr. Yasemin Yüksel Durmaz for her motivation and encouragement from the very beginning of my studies. I will not forget her efforts to find an advanced computer at our faculty for the simulations of my finite element model studies.

Last but not least, I would like to thank my family members, my parents and my brother, for their endless support, motivation, insightful comments, and enthusiasm throughout my life.

Saliha Zeyneb AKINCI

June, 2022

CONTENTS

Page

LIST OF FIGURES

LIST OF TABLES

LIST OF SYMBOLS

ρ : bone density
E : elastic modulus
υ : Poisson's ratio

ABBREVIATIONS

3D	:Three Dimensional
CT	:Computed Tomography
FEA	:Finite Element Analysis
FE	:Finite Element
MRI	:Magnetic Resonance Imaging
2D	:Two Dimensional
stp (step)	:Standard for The Exchange of Product Model Data
ROM	:Range of Motion
HU	:Hounsfield Unit
ASD	:Adjacent Segment Disease
CAD	:Computer-Aided Design
DICOM	:Digital Imaging and Communications in Medicine
PEEK	:Polyether Ether Ketone
ALL	:Anterior Longitudinal Ligament
PLL	:Posterior Longitudinal Ligament
ISL	:Interspinous Ligament
SSL	:Supraspinous Ligament
LF	:Ligamentum Flavum
ITL	:Intertransverse Ligament

ADOLESAN İDİYOPATİK SKOLYOZ HASTALARININ OMURGA İMPLANTLARININ MEKANİK ANALİZİ

ÖZET

Saliha Zeyneb AKINCI

Biyomedikal Mühendisliği ve Biyoenformatik, Doktora

Tez Danışmanı: Prof. Dr. Yunus Ziya ARSLAN

Haziran, 2022

Omurga implantları, omurga cerrahisindeki füzyon işlemini kolaylaştırmak ve omurganın eğriliğini düzeltmek için kullanılmaktadır. Spinal füzyonda, uygulanan biyomekaniksel baskı kuvvetleri modeldeki komşu segmentleri de etkilemektedir. Bu nedenle omurga implantlarının cerrahi müdahalesi, komşu segment hastalığı gibi omurga rahatsızlıklarına neden olmaktadır. Bu çalışma, lomber omurga modelindeki sabit pedikül vida sisteminin biyomekanik etkilerini araştırmaya odaklanmıştır. Bu amaçla, fonksiyonel omurga ünitesi modeli, adolesan idiyopatik bir hastanın bilgisayarlı tomografi görüntüsünden elde edilmiştir. Fonksiyonel omurga modeli, omurganın ikinci (L2) ve üçüncü (L3) omurlarından, iki tane faset eklemden, bir tane omurlararası diskten ve bunlara karşılık gelen ligamentlerden oluşturulmuştur. L2-L3 lomber modeli üzerindeki gerilme analizini incelemek için bir titanyum vida sabitleme sistemi oluşturulmuştur. Pedikül sabitleme sistemlerinin olduğu ve olmadığı L2-L3 modellerine 500 N basma kuvveti ve 8 Nm moment uygulanmıştır. Sonlu elemanlar analizi sonuçlarına göre, sabit implant sisteminin varlığının uygulanan basma kuvvetlerinin ektansiyon, yanal bükülme, eksenel rotasyon ve fleksiyonu da içeren dört yönlü hareketlerde, vidalara ve çubuklara dağıtılmasına olanak sağladığı sonucuna varılmıştır. Ayrıca, modeli sabitleyerek, von Mises gerilme değerleri implantlı sistemde azaltılmıştır. Sonuçlar, üstteki omurun (L2) en üst yüzeyinin, yükleme koşulları altında özellikle fleksiyon ve yanal bükülmede en çok etkilendiği bölge olduğunu göstermektedir. Buna ek olarak, lomber omurganın pedikülleri bu bölgelerin aksiyal rotasyon ve ekstansiyon hareketlerinde en çok etkilenen parçalar olduğunu göstermektedir. Bu sebeple, sonuçlar sabit implant sisteminin, omurganın kararlılığını sağladığını ve gerilme dağılımlarının komşu segmentlerde, özellikle de omurlararası diskte (L2-L3) azaldığını göstermiştir.

İkinci olarak, L2-L5 lomber omurga modeli de bütün gerekli omurga bileşenleri ile birlikte bu çalışmada oluşturulmuştur. CT tarama verisi bir önceki model için kullanılan ile aynıdır. Bu model dört tane lomber omurdan, üç tane omurlararası diskten, altı tane faset eklemden ve omurga ligamentlerinden oluşmaktadır. Aksiyal baskı kuvveti 800 N ve uygulanan moment 10.6 Nm'de tutulmuştur. L2-L5 modeline yerleştirilen omurga implantlarının malzeme özellikleri titanyum ve polyether ether ketone (PEEK) malzemeleri için karşılaştırılmıştır. Yükleme koşulları altında, L2-L5 lomber omurga modeli hem titanyum tabanlı, hem de PEEK tabanlı implant sistemlerinde, özellikle omurlararası disklerde ve pedikül vida sistemlerinde olacak şekilde, gerilme dağılımları göstermiştir. Komşu segment hastalığının etkilerini anlayabilmek adına, bir önceki L2-L3 modelinde olduğu gibi L2-L5 modelindeki omurlararası diskler araştırılmıştır. Bu iki

sabitleme sisteminin sonuçları karşılaştırıldığında, von Mises gerilme dağılım değerleri sabit omurga implant ile belirli bir oranda düşmüştür. Buna ek olarak, PEEK tabanlı sistem, daha da düşük toplam deformasyona ve eş gerilme dağılımlarına yol açmıştır. Modeldeki düşük gerilme değerleri özellikle L3-L4 ve L4-L5 omurlararası disklerde kaydedilmiştir.

Anahtar sözcükler: Sonlu eleman analizi, gerilme analizi, vida sabitleme sistemi, komşu segment hastalığı.

MECHANICAL ANALYSIS OF SPINAL IMPLANTS IN PATIENTS WITH ADOLESCENT IDIOPATHIC SCOLIOSIS

ABSTRACT

Saliha Zeyneb AKINCI

Ph.D. in Biomedical Engineering and Bioinformatics

Advisor: Prof. Dr. Yunus Ziya ARSLAN

June, 2022

Spinal instruments have been employed to facilitate the fusion processes in spinal surgeries and correct the misalignment of the spine. In spinal fusion, the compressive biomechanical forces applied to the models also affect the adjacent segments of the model. Thus, the surgical adjustments of the spinal implants can lead to spinal disorders like adjacent segment disease. This study is focused on the investigation of the biomechanical effect of a fixed pedicle screw implant system on the lumbar spine models. First of all, the functional spinal unit model was reconstructed from computed tomography scan data of an adolescent idiopathic scoliosis patient. The second (L2) and third lumbar (L3) vertebra, two facet joints, an intervertebral disc, and the corresponding ligaments were all constructed in this study. A titanium screw fixation system was used to investigate the stress analysis on the L2-L3 lumbar model. 500 N compressive load and a moment of 8 Nm were applied to the L2-L3 models with and without the screw fixation systems. According to the results, it was concluded that the existence of the fixed implant system allowed for the transmission of the applied compressive loads to the screws and rods in the model in four directional movements including extension, lateral bending, axial rotation, and flexion. Also, by stabilizing the model, the von Mises stress values were decreased with the implanted system. The results showed that the top surface of the upper vertebra (L2) was the most affected region, especially in flexion and lateral bending under loading conditions. Additionally, the pedicles of the lumbar vertebrae indicated that these regions were the most affected parts in axial rotation and extension movements. Therefore, the results showed that the fixed implant system provided the maintenance of the model and decreases the stress distribution on the adjacent components, especially on the (L2-L3) intervertebral disc of the model. Secondly, the L2-L5 lumbar model was also constructed with all the relevant spinal components in this study. The CT scan data was the same as used for the previous model. The finite element model is constituted of four lumbar vertebrae, three intervertebral discs, six facet joints, and the spinal ligaments. The axial compression force was 800 N and the applied moment was kept at 10.6 Nm. The material properties of the spinal implants that were inserted into the L2-L5 model, were compared for titanium and polyether ether ketone (PEEK) materials. Under the loading conditions, the L2-L5 lumbar model showed the stress distributions especially on the intervertebral discs and pedicle screw implant systems both for the titanium and for the PEEK-based spinal implants. To understand the effects of the adjacent segment disease like the previous L2-L3 model, the intervertebral disc structures of the L2-L5 model were investigated. According to the comparison results of these two fixation systems, the von

Mises stress distribution values were decreased to a certain value with the fixed-based implanted system. And also, the PEEK-based system led to lower total deformation and equivalent stress distribution. The lower stress values of this situation were recorded especially on the L3-L4 and L4-L5 intervertebral discs of the model.

Keywords: Finite element analysis, stress distribution, screw fixation system, adjacent segment disease.

CHAPTER 1

1. INTRODUCTION

The spine, also known as the vertebral column, is constituted of bones and soft tissues such as vertebrae, joints, tendons, ligaments, intervertebral discs, and muscles. Since it is the center of the skeleton, it plays an important role in the transmission of forces, weights, and moments through body movements. This dynamic structure functions correctly with all the corresponding bones, ligaments, nerves, and muscles, and this complex system allow the vertebral column to make flexion, extension, right lateral bending, left lateral bending, and axial rotation. Besides, this dynamic flexible property of the system also protects the spinal cord of the vertebral column from neural injuries [1], [2].

Scoliosis is an abnormal deformation of the vertebral column [3]. This three-dimensional misalignment of the spine gradually causes degeneration of the soft tissues like intervertebral discs and facet joints, especially in the lumbar and thoracic spine regions of the patients [4]. According to biomechanical studies, it has been concluded that when loading conditions have been applied to the intervertebral disc areas, the deformation of the vertebral column has decreased. As a result of this situation, stabilization of the spine has been investigated with various corrective forces [5]. To decrease the deformation and the pain of the patients, spinal fusion is the most used method to correct the abnormal curvature of the spine. This surgical procedure has been applied to the spine by the insertion of screws and rods into the vertebrae [6].

The objectives of this study involved the investigation of the biomechanical effects of the fixed pedicle screw fixation systems on lumbar spinal models. The finite element (FE) lumbar models of L2-L3 (the model between second and third lumbar vertebrae) and L2-L5 (the model between second and fifth lumbar vertebrae) were developed and a fusion of rigid rod and pedicle screw fixation system was employed for the simulation process of each of these spine models. Also, the efficacy of the PEEK (polyether ether ketone)-

rod implant system was investigated in this study. The comparison of the von-Mises stress distribution results was compared with the traditional titanium-based pedicle screw fixation system.

1.1. Literature Review

The human spine is capable of performing various motions and can endure carrying heavy loads during physical movements [7]. Spinal damages affect numerous adjacent segments. Thus, the comparison of the effect of different fixation techniques involving the spinal diseases that are composed of various adjacent segments is very important [6].

The treatment of scoliosis largely depends on the medical instrumentations and the experience of the surgeons in this field [8]. This deformation of the vertebral body needs to be corrected by the application of certain loads and spinal instruments have been employed to correct these abnormalities of the spine [5].

The evaluation of the deformity of the vertebral column under applied stresses and also examining the material features of the spinal structures are also important to understand and investigate the treatments of scoliosis [8], [9]. As a result of the developments of material properties in spinal instrumentation, improvements in deformity correction studies have increased. When the mechanical strength in instruments is increased during scoliosis surgery, the acting force between bone and implant interface is improved [10].

In recent years, the rate of scoliosis, which is related to the degeneration of spinal components including the intervertebral discs, facet joints, bone, and ligaments, has been increasing [4]. The nerve roots of the spine are affected by the applied compressive forces and thus, it can be painful for the patients to endure this back pain. Therefore, spinal surgery is the most common option to decrease this neurologic pain [6] for patients with severe or progressive deformities in order to decrease the angle of the deformity of the spine [5]. The degeneration of the intervertebral disc and facet joints causes the spinal column to align in the coronal plane [4].

Researchers have studied in vivo to find out the spinal muscle forces and internal loads by calculating the pressure in the intervertebral discs or measuring the loads on the fixation systems. Since biomechanical models are the result of non-invasive approaches, they have been used to determine muscle forces and passive components of the human trunk [11].

In the treatment of spinal diseases, the combination of transforaminal lumbar interbody fusion with bilateral pedicle screw has been commonly used. This method allows to decrease the complications in the post-operative time and also supports the recovery period of the patient. On the other hand, excessive spinal muscles in the surgical area may be damaged by the dissection during spinal instrumentation. Additionally, the degree of stiffness can be increased as a result of the rigidity of this fixation system. In order to solve this problem, a unilateral pedicle screw has been employed as an alternative fixation system [6]. Although a unilateral pedicle screw decreases the spinal stability when compared with a bilateral pedicle screw, it might be a problem during bending and rotation. An alternative internal fixation technique has been used to overcome this problem. A contralateral translaminar facet screw has been employed. This method improves spinal stability and increases the effectiveness of the internal fixation [6].

Zahaf and Kebdani studied the mechanical behavior between rigid and dynamic fixation systems of the spinal column of two lumbar vertebrae with finite element analysis (FEA). To clarify the effectiveness of each design, the comparison was done between rigid and dynamic fixation systems on a two-segment spinal model. The lumbar model was subjected to the maximum possible load for all physiological motions; anterior load (flexion), posterior load (extension), lateral load (flexion lateral), and axial load (torsion) [12]. The finite element method (FEM) was employed to demonstrate the von Mises stress distribution in the disc area and also to understand the overall displacement of the segment during physiological movements [12]. Zheng et al. developed and validated a three-dimensional FEM of the spine as well [4]. Little et al. investigated the effect of various surgical corrective forces on deformity correction [5]. Abe et al. studied the prospective corrective forces and pull-out forces using FEA [10]. The group developed a new method as an estimation of the corrective forces by analyzing the geometrical change during spine surgery. In addition to corrective forces, pull-out forces were also investigated on the pedicle screws with the help of FEA [10].

The pedicle screw fixation system protects the structure of supraspinous and interspinous ligaments. This fixation system consisted of two rods and pedicle screws [12]. The intervertebral disc contributes to flexibility and mobility of the mechanical behavior of the spine [7]. However, adjacent segment disease (ASD) has become a common drawback of fusion surgeries. In order to decrease the degree of this pathology in theory, novel motion preservation methods have been developed. This degenerative change in the

spinal column adjacent to a region that is treated surgically has several obvious symptoms including radiculopathy, myelopathy, or instability [13]. There are many studies about adjacent disc degeneration and ASD. Researchers have tried to find the answer whether they are the results of natural aging because of degeneration or they are the results of adjacent segment fusion and its related changes [13].

1.2. Finite Element Analysis and Its Applications In Spine Research

The FEM, which was developed in the 1900s, is a numerical technique to solve various engineering approaches including steady-state, linear or non-linear, stress or strain analysis, fluid mechanics, or heat transfer problems [14]. Because of the lack of the limitations of the traditional biomechanical testing, FEA allows researchers to control all the parameters of the study. Also, the applied forces and the stresses produced internally can all be evaluated with this method, too [4]. Therefore, this method has been commonly used in spinal biomechanics. Since spinal components have irregular geometries with non-linear responses and non-homogeneous materials, this technique has been considered a suitable option for computational modeling [15]. Moreover, it allows the users to understand the differences between healthy and degenerated spines of individuals. Also, the investigation of the effects of various spinal instruments on spinal performance can be evaluated with this approach. As a result of the assessments of the spinal instrumentations, new implants can be designed and developed [15], [16].

There are subdomains of structure in FEM. Finite number of elements that connect the related nodes are used to represent each subdomain in the structure. Thus, this method enables researchers to obtain the complex structure of the whole model accurately [8].

In spine biomechanics, computed tomography (CT) scan data has been employed to obtain subject-specific models of bone structures for FEA [17] and to investigate the deformation of the spine. The effect of the stress distribution on the spine can also be examined with this technique [7]. All spinal components including cortical and cancellous bones, facet joints, and posterior elements can also be obtained by using the solid elements in the modeling [8]. The understanding of the mechanics of scoliosis can also be enhanced with the help of FEM [8].

CHAPTER 2

2. THEORETICAL PART

2.1. Biomechanics of The Spine

The vertebral column consists of several sections, and these sections involve a different number of vertebrae. These regions and the number of vertebrae of that regions are the cervical region (7 vertebrae), thoracic region (12 vertebrae), and lumbar region (5 vertebrae, 5 fused sacral vertebrae, and 3-4 fused coccygeal segments) [2], [18].

The spine has different curve structures in each of these regions. The cervical and lumbar spine are convex anteriorly and, the thoracic and sacral spine regions are convex posteriorly [19]. If the spine and its components are damaged by any kind of injury, spinal disease, or strain, then this will affect the whole vertebral column and lead to severe back pain [20].

If there are structural abnormalities in the spine, then the natural curve form of the vertebral column is altered. When the spine is bent backward, the curve is called lordosis, and if it is bent forward, it is known as kyphosis. The other structural abnormality of the spine is scoliosis [2]. In **Figure 2.1**, the CT image of a scoliotic patient is seen. The deterioration of the alignment of the vertebral column can be seen especially in the middle region of the spine. This region of the scoliotic curve is the location of the thoracic region. This region of the spine has a crucial role directly in the sympathetic nervous system of the body by protecting the inner organs like the lungs and heart. If this region does not function properly, then spinal damage can affect the whole spinal structures of the thoracic spine and also can negatively affect the mobility of the patient [2], [3], [21].

The abnormal condition of the spine and rotation of the vertebral column can be seen if the deformity of the spine is in the frontal plane. This misalignment can be detected by imaging methods such as CT, X-rays, magnetic resonance imaging (MRI), or by

examining the condition of the patients. Surgical procedures have been applied according to the condition of the curvature of the spine [1], [2], [21].

To deliver the applied loads and forces equally through the vertebral column, the correct alignment of the spine should be preserved. In these circumstances, orthopedic surgeons have used spinal instrumentation techniques to maintain the normal alignment of the spine by stabilizing it. The mechanical features of these spinal instruments can be changed according to their stress-strain, fatigue, and tensile strength properties. Thus, the equal load sharing of the vertebral column can be seen after this stabilization [1].

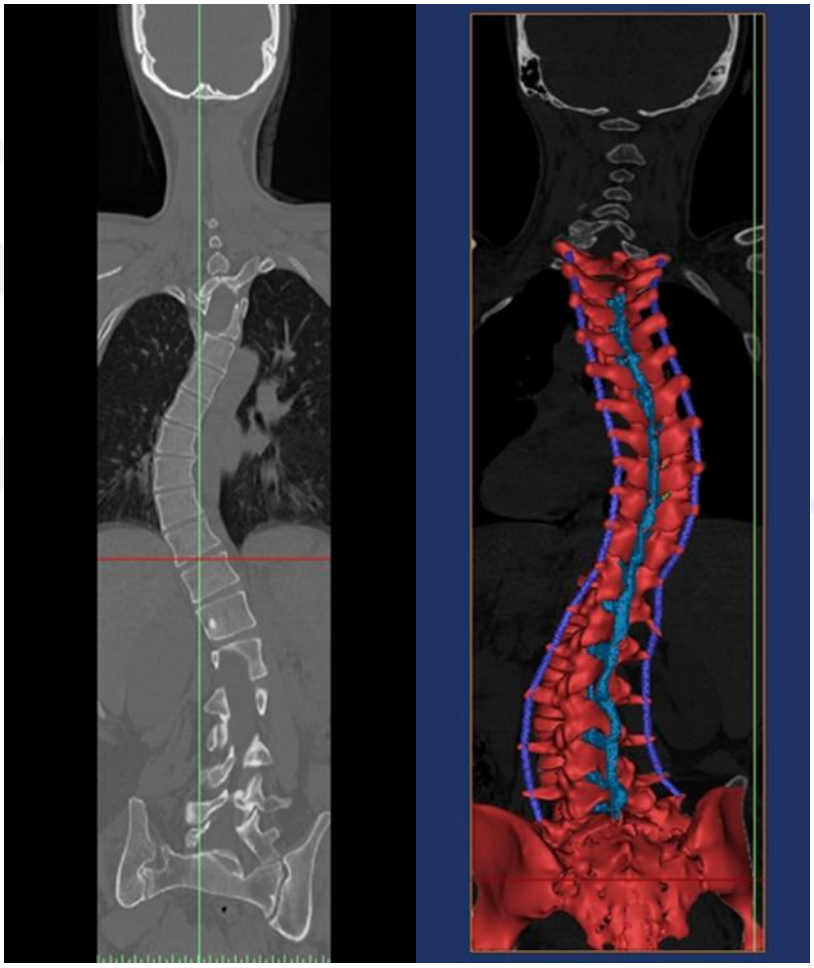

Figure 2.1: The CT image of a scoliotic patient (left) and the three-dimensional (3D) model of the whole spine (right). All the spinal components are seen in different colors. Vertebrae, intervertebral discs, and facet joints are represented in red, and the corresponding ligaments are seen in blue and purple colors [22].

2.1.1. Structure of the vertebrae

There are structural differences between different vertebral bodies in each region of the spine including cervical, thoracic and lumbar sections. Although they seem to be similar, they have significant differences from each other. Each vertebral body involves the main

body and corresponding sections that are depicted in **Figure 2.2** as pedicles, vertebral arch, transverse process, superior articular processes, spinous process, and lamina. The structural differences are given in **Figure 2.3** showing the vertebral bodies of the thoracic (T2-T12) and lumbar spine (L1-L5) regions. The anatomical features of the lumbar spine are different from the thoracic vertebrae. Lumbar vertebral bodies from L1 to L5 have larger bodies and weight than the other vertebrae in the spinal column.

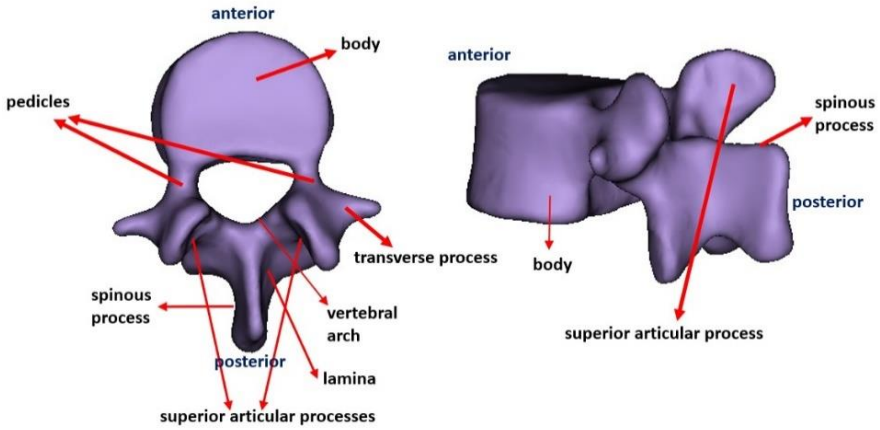

Figure 2.2: The structure of a vertebra and its various processes [22].

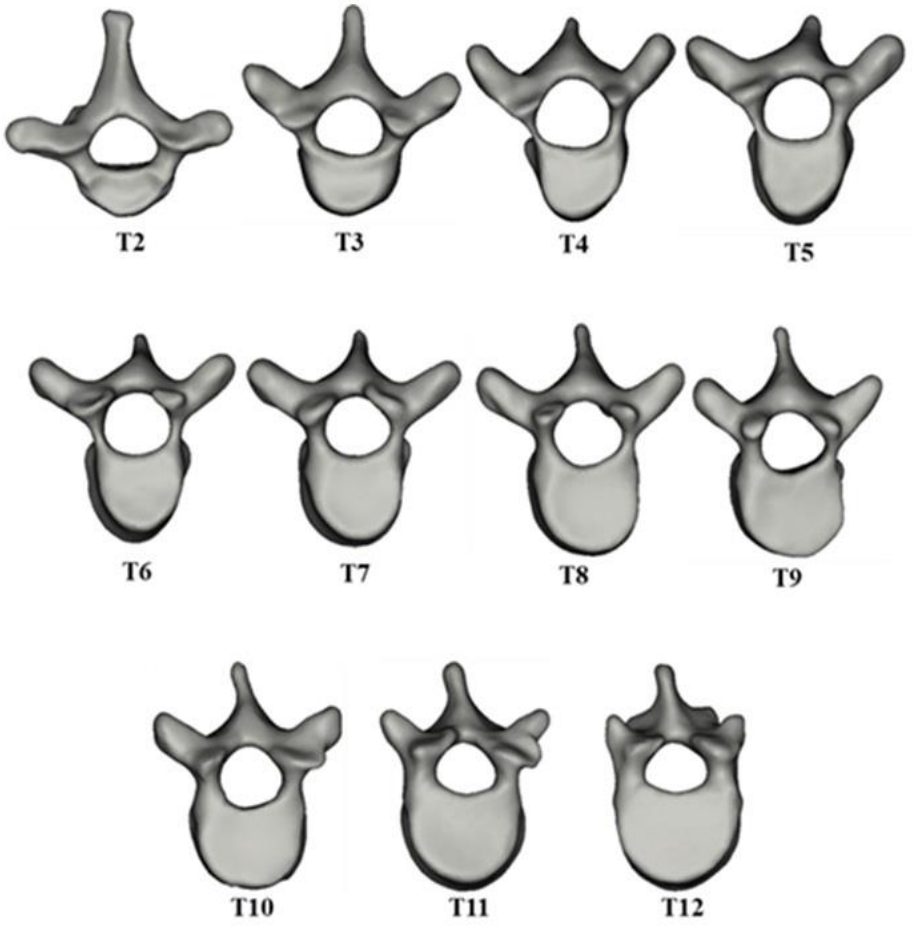

(a)

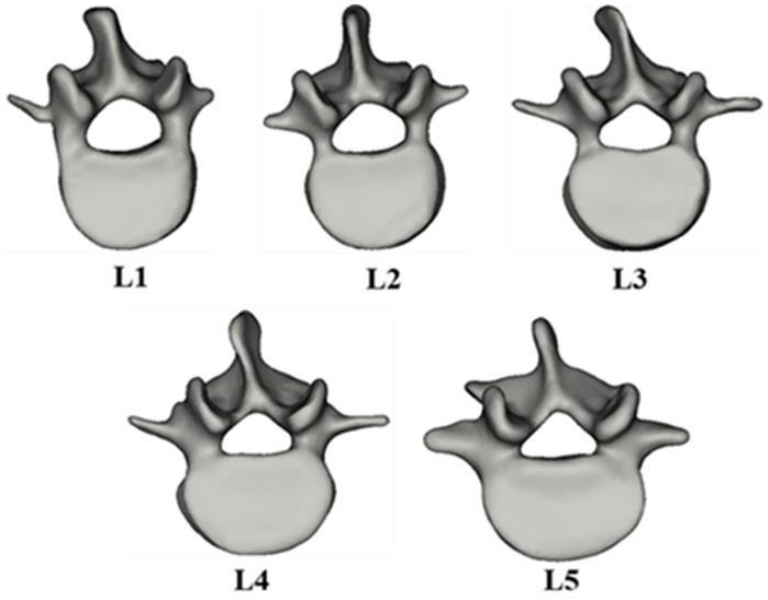

(a)

Figure 2.3: The depiction of the (a) thoracic vertebrae (T2-T12) and (b) lumbar vertebrae (L1-L5) of the spinal column [22].

2.1.2. Structure of the intervertebral disc

In a normal healthy spine, the intervertebral disc is the center that absorbs and resists all the loads that are applied through the vertebral column [15]. Also, it is a complex structure with water, matrix proteins, and proteoglycans which maintain flexibility in the spine [23]. The disc structure involves the nucleus pulposus, the annulus fibrosus, and endplates. In **Figure 2.4**, the three-dimensional view of the full disc structure is given.

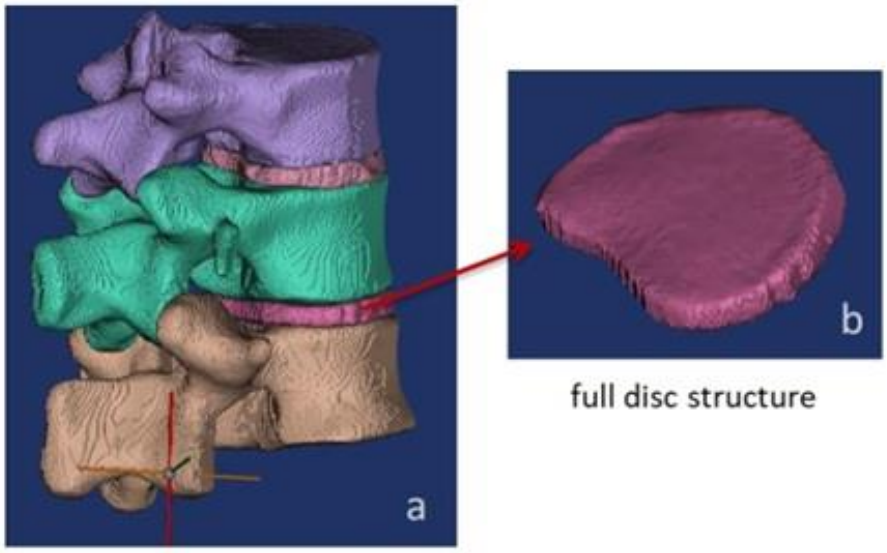

Figure 2.4: (a) The 3D view of the spine model with corresponding disc structures, (b) the intervertebral disc between vertebral bodies [22].

2.1.3. Structure of the facet joint

The significant anatomical properties of the facet joint structure have an important role in the mechanical behavior of the spine. They are placed between two posterior parts of the two vertebrae. The placement of each pair of the facet joints is given in **Figure 2.5**. This figure shows the 3D models of the joint structures and the corresponding spinal components. If the spine is not damaged or degenerated, then the facet joints promote the mobility of the movement of the spinal column with lower friction forces [24].

While the direction of the facet joints is in the vertical direction in the thoracic spine, they are slightly parallel to the upper spinous processes in the lumbar region. Besides, these joints have different orientation angles in each human spine [15].

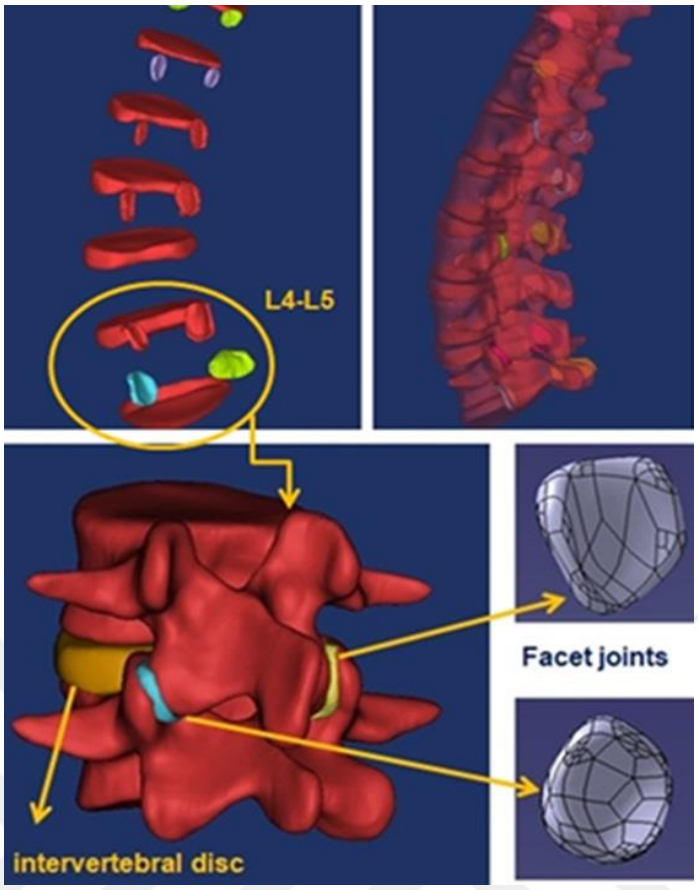

Figure 2.5: The direction of a pair of facet joint between the lumbar vertebrae and the 3D view of the facet joints and the related spinal components [22].

2.1.4. Structure of the ligaments

The biomechanical structure of the spine maintains the stability of the spinal column against structural abnormalities [2], [18]. The functionality of the whole spine is preserved by the strong fibrous structures, also known as the ligaments. They support the whole spinal components from external effects [2], [25]. The major ligaments in the spine are ligamentum flavum, and anterior and posterior longitudinal ligaments (**Figure 2.6**). These structures improve the stability of the spine and behave like a limiting factor for excessive movement of the spinal column [26].

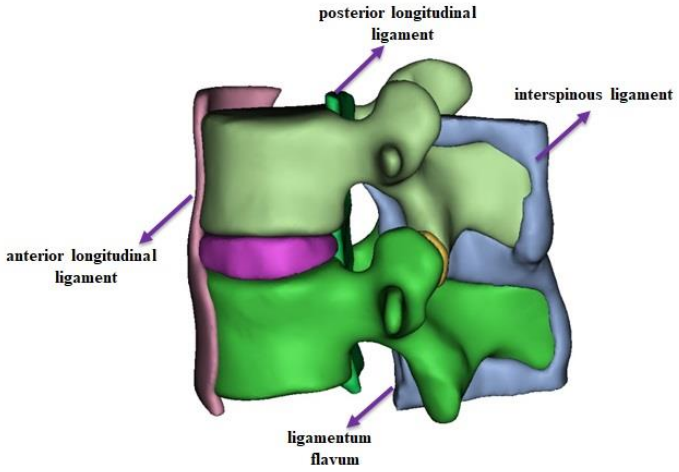

(a)

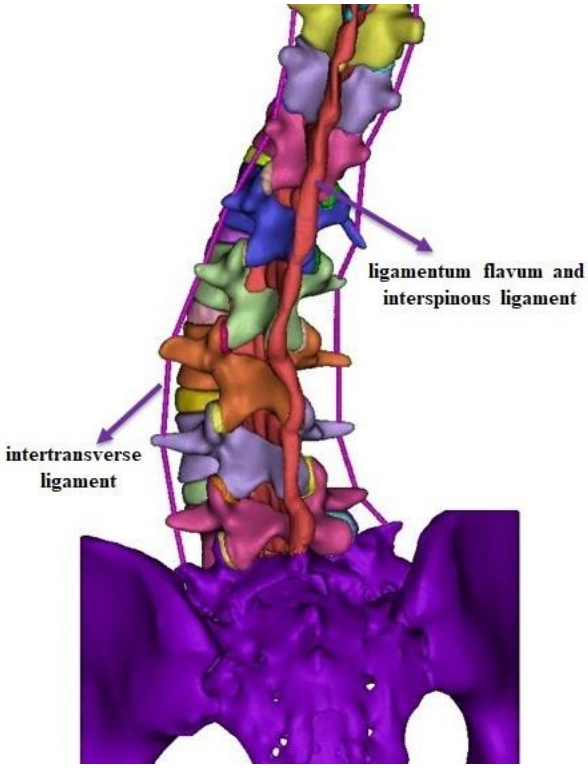

(b)

Figure 2.6: The representation of spinal ligaments (ligamentum flavum, anterior and posterior longitudinal ligaments) in the (a) L2-L3 model, and (b) in the model of T10-Sacrum [22].

Besides, anterior and posterior longitudinal ligaments hold the spinal components together and preserve this situation by limiting the excessive motions of the spine. The other major ligament that has a role in providing stability is the ligamentum flavum. This ligament is placed between adjacent spinous processes of the vertebrae [2], [25].

2.2. Construction of Spine Models

2.2.1. Segmentation and reconstruction of spine models

CT is an imaging technique that has been employed to diagnose spinal injuries. This method is based on the measurement of absorption/attenuation of tissues under the effect of radiation. The bone density of the CT scan images can be determined according to the Hounsfield unit (HU) values of that two-dimensional image. Thus, the difference in the densities between two sections of the bones allows them to be assigned as cancellous and cortical sections [27].

The FE modeling of the spinal instruments begins with image segmentation. After this step, reconstruction of the structures as 3D models can be obtained. Before the FEA of the models, mesh generation and appropriate material assignment should be completed [28].

In order to define the exact geometry of spinal components, CT scan images of patients or human cadavers have been employed [29]–[33]. Since many methods have been used to determine the correct geometries of the spinal instruments [30], the development process has been gradually improved step by step as represented in **Figure 2.7**.

Firstly, an appropriate image processing software (Mimics (Materialise's Interactive Medical Image Control System, Belgium), 3D Slicer, 3D Doctor, or Vesalius3D) should be used for the segmentation of the CT scan images [29], [33].

After completing the segmentation process, the reconstructed 3D images can be obtained [28], [29]. Following this step, meshing should be done to all the reconstructed models. For this purpose, suitable analysis software should be chosen for finite element analysis such as Abaqus/CAE or Ansys Workbench (Ansys Inc. Canonsburg, PA, USA) [15].

Additionally, modeling methods for orthopedic structures can also involve MRI scans for the spinal components that are not recognized from CT images [29].

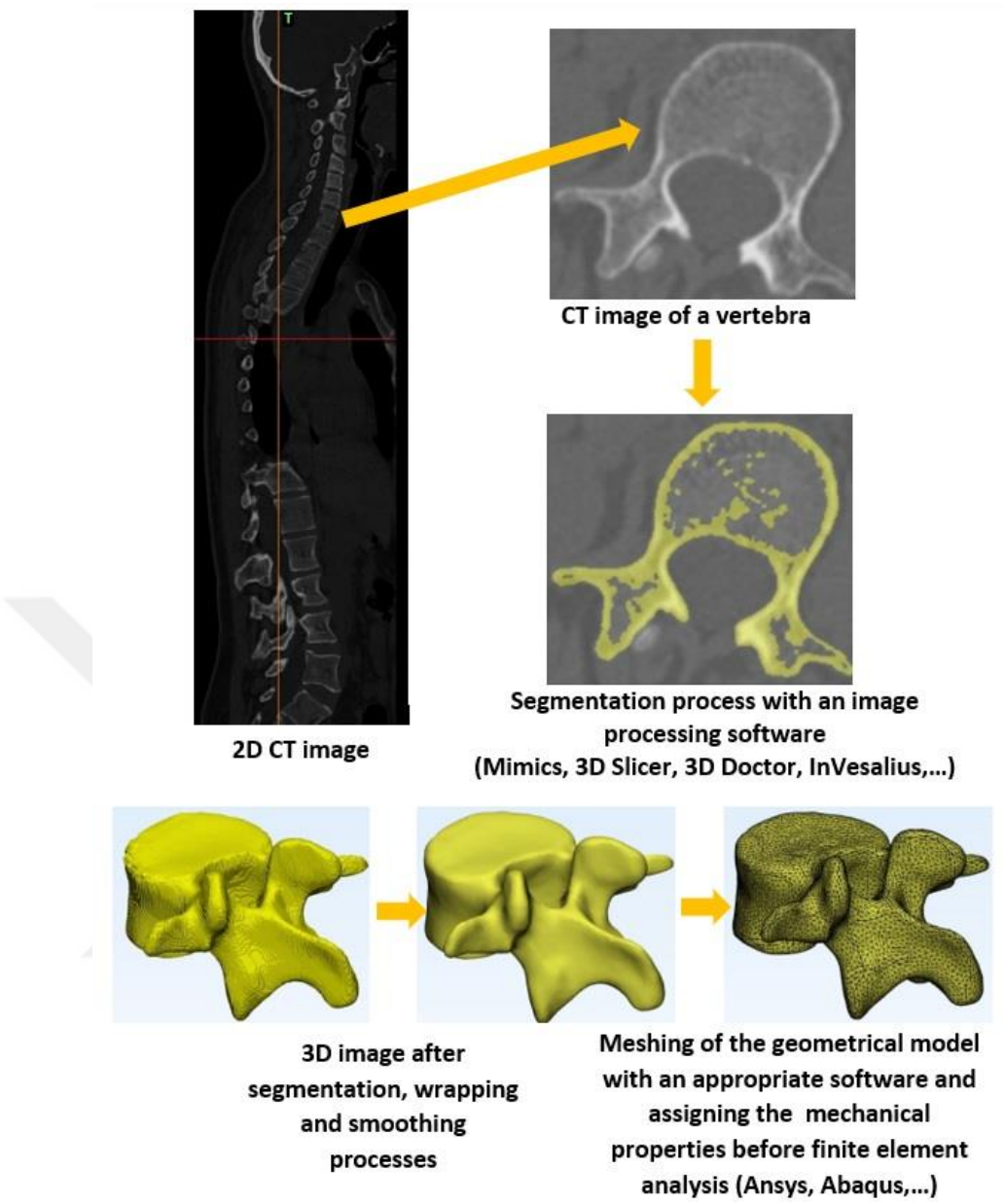

Figure 2.7: The modeling steps of a vertebra starting from the CT scan data to the meshing of the 3D view of this structure [22].

The file type of CT images is DICOM (Digital Imaging and Communications in Medicine) in the modeling stage. This scan data is being processed in the medical imaging software to reconstruct the relevant anatomical structures. Once the solid model construction and surface improvements have been finished, the meshing is applied to the objects of the model. **Figure 2.8** shows the comparison of the surfaces before and after the surface enhancements without altering the details of the vertebra. The improved surface mesh has a smoother surface and finer mesh; thus, it is much better for finite element analysis [34].

In the meshing part of structures, there are various types of elements including tetrahedral,

wedge, and hexahedral employed in biomechanical studies [34]. After assigning appropriate elements, the spinal models can be ready for the simulations in a suitable finite element software [28].

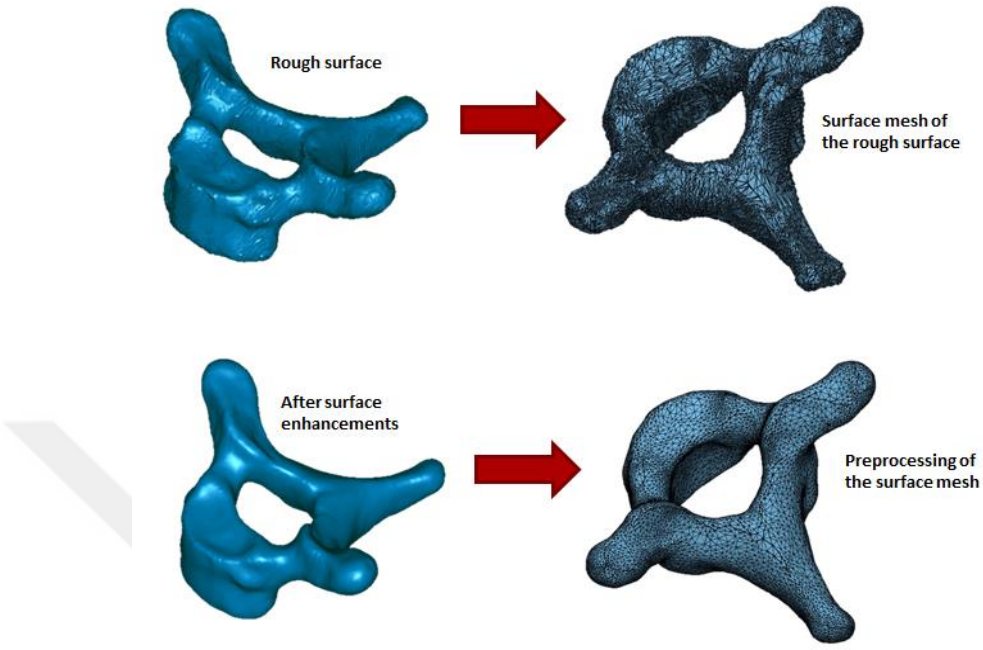

Figure 2.8: The comparison of the surface mesh before and after the surface enhancements. The improved surface mesh has a smoother surface and finer mesh for further analysis [22].

2.2.2. Material assignment in spine models

In the segmentation process, HU threshold values have been used to reconstruct the 3D bone images in the medical imaging software [35]. These values are dimensionless and have standardized forms of images. In CT imaging, different tissues of the human body have their own HU values concerning their density values at the grayscale level. For example, the air has a HU value of -1000 and water has a 0 HU value. This value is greater than 1000 for the bone tissues in CT scan data [36]. Therefore, measuring the HU values has been used to analyze the bone quality in CT scan data in terms of strength and density of the bone [36], [37].

After the segmentation process, the dimensionless HU values have also been used to assign mechanical properties to the bone tissues. The two layers of the vertebral bone have different HU values. For the cancellous bone, HU values are between 200-500. The bulk density of this region is between 0.75-0.97 g/cm^3 [38].

In addition to this, the cortical bone can also have a different HU range which is higher than 700 HU. According to another group, the HU value for the cancellous bone is associated with less than 700 HU [39].

The relation between HU and bone density is given by the following formula:

$$\rho = 1.122 \quad HU + 47 \qquad \textbf{(1)}$$

Several biomechanical studies involve only one elastic modulus value for the rest of the model, however, in order to get a more accurate spine model, two different bone segments (both for the cortical and the cancellous bones) should be considered [40]. In order to define this difference between two different bone tissues, the appropriate elastic modulus values can be employed as given in the following equations (**Eqs 2 and 3**) [38].

$$E_{cancellous} = 1.904 \ x \ \rho^{1.64} \qquad \textbf{(2)}$$

$$E_{cortical} = 2.65 \ x \ \rho^{3.09} \qquad \textbf{(3)}$$

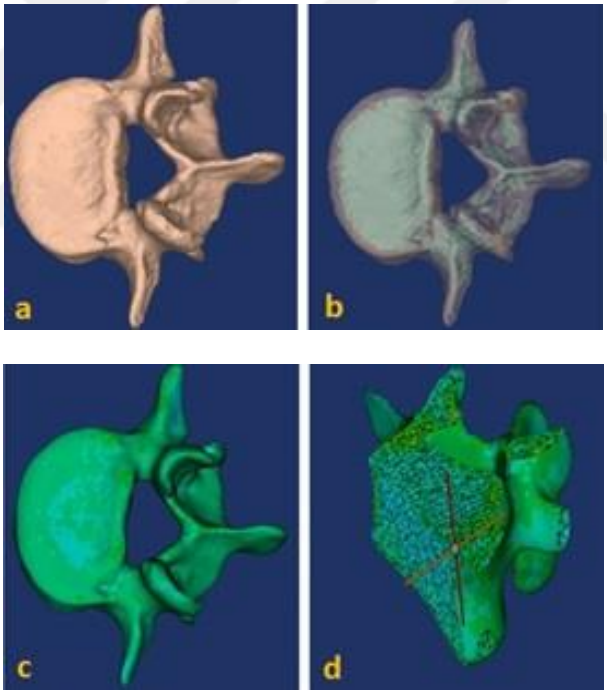

Figure 2.9: (a) The 3D view of the L4 vertebra. (b) The inner and outer shells of the bone can be noticed. The light green section indicates the cancellous bone region of the vertebra. (c-d) The clipped view of the bone after the assignment of the material properties [22].

The material assignment can be performed in medical imaging software. After the segmentation process, the obtained 3D objects are further edited by defining the volumetric meshes in these vertebral bone segments. Then, appropriate elastic modulus

and Poisson's ratio values can be assigned in the meshed bone structures. **Figure 2.9** indicates the steps of material assignments into a vertebra.

In the literature, there are various types of elements, modulus of elasticity, Poisson's ratios, and also the cross-section areas of the spinal components employed in FE modeling of the spine models. **Table 2.1** represents these spinal structures and their material properties.

Table 2.1: Element types and material properties of the spinal structures in FE modeling of the spine.

Spinal structure	**Element type**	**Modulus of elasticity (E) (MPa)**	**Poissons's ratio (υ)**	**Thickness of the cross-section area (mm^2)**
Cortical bone	6 node points triangular facet shell element [4] hexahedral element [41] 4-node shell [5] volumic (solid) [42] shell element [43]	11300 [5] 10000 [41] 12000 [4], [6], [12], [42]–[44]	0.2 [5] 0.3 [4]–[6], [12], [42]–[44]	
Cancellous bone	10 node points tetrahedron solid element [4] tetrahedral element [6] hexahedral element [41] 8-node brick element [5] volumic (solid) [42] tetrahedral element [43]	140 [5] 100 [4], [6], [12], [42], [43] 450 [41]	0.2 [5], [6], [12], [42], [43] 0.3 [4] 0.25 [41]	

Lamina terminalis	10 node points tetrahedron solid element [4]	4000 [4]	0.4 [4]	
Ground mass of the annulus fibrosus (disc annulus)	10 node points tetrahedron solid element [4] hexahedral, 8 nodes (hyperelastic, incompressible) [45] hexahedral element [5], [6]	4.2 [4], [6], [12], [41], [42]	0.45 [4], [6], [12], [41], [42]	
Annulus (fiber)	2 node points cord element [4] rebar [41] 8 node brick [5]	450 [41] hyperelastic, Mooney-Rivlin (C_{10} = 0.7, C_{01} = 0.2) [5]	0.3 [41]	
Nucleus pulposus	10 node points tetrahedron solid element [4] hexahedral element (incompressible fluid) [6] incompressible fluid element [41] 4- node hydrostatic fluid (incompressible) [5] 8-noded brick [15] 8 nodes brick element (isotropic, elastic) [46]	4 [4] 1 [6], [12], [15], [41], [44] 2 [46]	0.49 [4], [6] 0.499 [12], [15], [41], [44], [46]	
Articular cartilage	10 node points tetrahedron solid element [4]	1000 [4]	0.3 [4]	

Contact face of the superior articular process	6 node points triangular facet object element [4]			
Contact face of the inferior articular process	6 node points triangular object shell element [4]			
Anterior longitudinal ligament (ALL)	tension only, truss elements 2 node spring [41] 2 node points cord element [4] 2 node spring element [5]	15 (<12%), 30 (>12%) [41] piecewise, non-linear elastic [5] 7.8 (< 12%), 20 (>12%) [12] 20 [6] 7.8 [47]	0.3 [12], [41], [47] 0.4 [6]	11.1 [41] 75.9 [4] 66 [47]
Posterior longitudinal ligament (PLL)	2 node points cord element [4] tension only, truss elements [41] 2 node spring element [5]	10 (<12%), 20 (>12%) [41] 20 [6] piecewise, non-linear elastic [5] 10 (<11%), 20 (>11%) [12] 10 [47]	0.3 [12], [41], [47] 0.4 [6]	51.8 [4] 11.3 [41] 26 [47]
Ligamentum flavum (LF)	2 node points cord element [4] tension only, truss elements [41]	15.0 (<6.2%), 19.5 (>6.2%) [12] 5 (<25%), 10 (>25%) [41]	0.3 [12], [41]	46 [41] 78.7 [4]
Capsular ligament (CL)	2 node points cord element [4]	7 (<30%), 30 (>12%) [41]	0.3 [6], [12], [41], [46]	102.5 [4] 42.2 [41]

	tension only, truss elements [41] tension only, truss elements (hypoelastic) [46]	7.5 (<25%), 32.9 (>25%) [12] 10 [6] 7.5 (<25%), 32.9 (>25%) [46]		
Intertransverse ligament (ITL)	2 node points cord element [4] 10 (<18%), 58.7 (>18%) [12] truss element [29]	10 [47] 10.0 (<18%), 58.7 (>18%) [29] 10 [7]	0.3 [29], [47]	40.5 [4] 2 [47] 0.3 [7]
Supraspinuos ligament (SSL)	2 node points cord element [4] tension only, truss elements [41] tension only, spring elements54	8.0 (<20%), 15.0 (>20%) [12] 4 (<20-40%), 8(>40%) [41] 8 [47]	0.3 [12], [41], [47]	75.7 [4] 13 [41] 30 [47]
Cartilage endplate	hexahedral element [41] shell element [43]	12000 [12] 3500 [41] 1000 [43]	0.3 [12], [43] 0.25 [41] 0.4 [44]	
Posterior bone	10 node-link elements (tension resistance only) [12]	3500 [12]	0.25 [12]	
Facet (apophyseal) joint	contact (GAP) element [15], [42] nonlinear soft contact, GAPUNI [41] shell element [43]	75 [43] 23.8 [44]	0.4 [43], [44]	

2.3. Modeling Studies of The Spine

2.3.1. Modeling of the vertebrae

From CT scan data, bony structures of vertebrae, including their posterior parts, can be constructed in the modeling stage. This process involves the segmentation procedure that is used to define the elements of posterior and vertebral body sections. Thus, segmentation is employed to separate different parts by deleting pixels of the related structure by using different segmentation masks. Additionally, dividing into different segments can be monitored in all plane regions including axial, coronal, and sagittal regions [15].

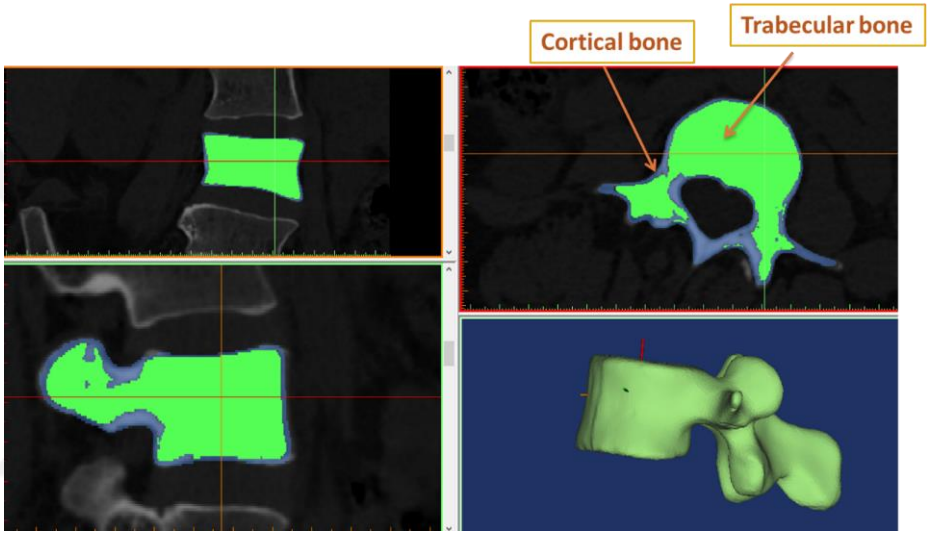

Figure 2.10: The segmentation procedure of a vertebral body that defines the cortical and cancellous regions [22].

In addition to the posterior parts, a vertebral body involves two sections as cortical and cancellous parts. To define these sections, specific shell elements can be used for meshing and analysis. An example of a segmentation procedure of a CT scan image is given in **Figure 2.10**. Different masks are describing the cancellous (trabecular) and cortical (the outer shell) regions of the bone. While the blue mask stands for the cortical part, the green one is for the trabecular region [4], [5], [41], [42], [48].

2.3.2. Modeling of the intervertebral discs and facet joints

Intervertebral discs between vertebral bones are the most vulnerable soft tissues of the spinal column. They can be damaged by spinal degeneration or excessive deformation [7], [45], [49].

In the construction of spinal models, there are many types of elements and materials used for the discs and joints in the vertebral column. Modeling of these structures involves different methods that have been used in various biomechanical studies [4], [7], [24], [47], [50]. The bone tissues can be detected from CT scans, however, the soft tissues like intervertebral discs and facet joints need to be manually segmented to define the separate components [51]. Manual segmentation of intervertebral discs and their inner layers with different masks is represented in **Figure 2.11**. Following this procedure, 3D objects of both facet joints and discs can be obtained.

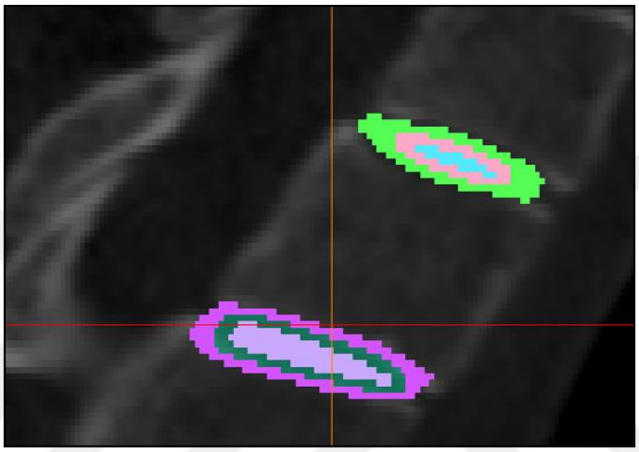

Figure 2.11: Segmentation procedure of an intervertebral disc and its inner surfaces with different masks manually [22].

Another method of manual segmentation is based on the loft operation in CAD software, for example, SolidWorks (Dassault Systemes, Massachusetts, USA), to define the space between the base of one vertebra and the top side of the other vertebra. A representation is given in Figure 2.12 for the lofted form of the intervertebral disc. The 3D image of the functional spinal unit and the corresponding disc structures with annulus and nucleus regions are shown (**Figure 2.12**).

According to the nature of the nucleus pulposus, incompressible viscoelastic material characteristics can be applied in the modeling section [52], [53]. Additionally, tension resistance material properties can also be used for the collagen fibers that are located with an angle of $\pm 30^{o}$ in the annulus region of the intervertebral disc [10], [11]. In addition to this, collagen fibers can also be developed by nodal displacements in the radial direction in the annulus region of the intervertebral disc. This manual creation method involves a circular type of mesh located between the endplates of the disc as concentric rings with an orientation of $\pm 30^{o}$ [11]. The rebar elements or truss elements can be used to mimic the modeling of the annulus fibers in the annulus region of the intervertebral discs [10].

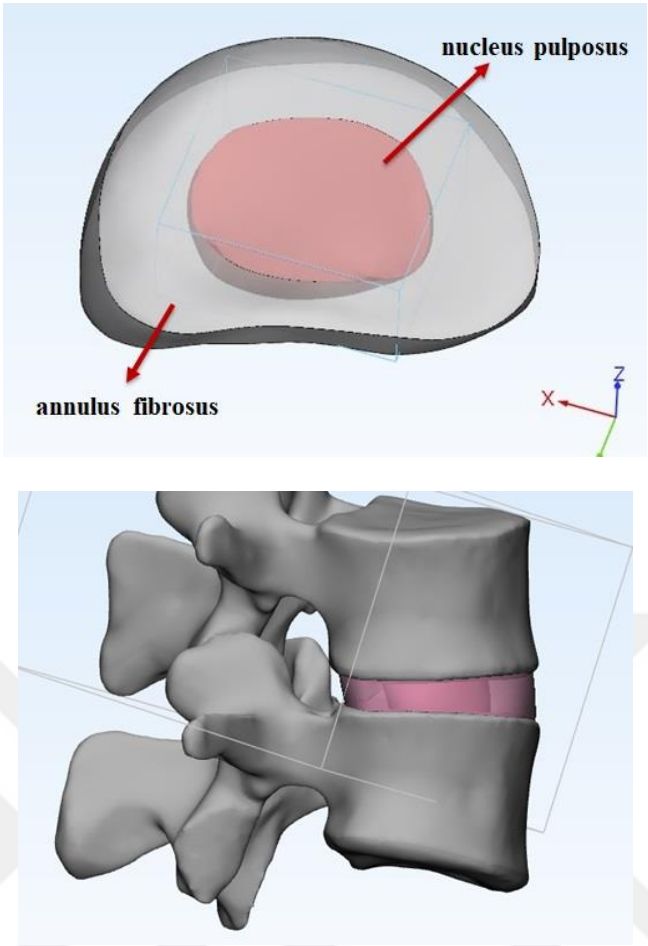

Figure 2.12: (a) The lofted form of the intervertebral disc with nucleus pulposus and annulus fibrosus, and (b) 3D view of the functional spinal unit with the disc structure [22].

The disc structures can also be modeled as surface node sets. The nodes that define the boundaries between the upper and lower part of the vertebrae, also indicate the regions for the splines that fitted onto these closed surfaces for the construction of the intervertebral discs [54].

The annulus fibers which can also have anisotropic hyper-elastic properties, can be modeled with the hexahedral type of elements. The annulus region can also be separated into three sections such as anterior, posterior, and lateral regions of the disc area [54]. The element type of the nucleus pulposus can be a fluid-filled membrane element in the intervertebral disc. Facet joints can be constructed by manual segmentation in medical imaging software. The development of facet joints between two adjacent vertebrae is represented in **Figure 2.13** in coronal, axial, and sagittal planes [54].

In the modeling procedure of facet joints, different element types have also been employed in the studies. For example, Bredbenner et al. used facet surfaces to define the facets as cartilages projected onto the adjacent areas of the surfaces [54].

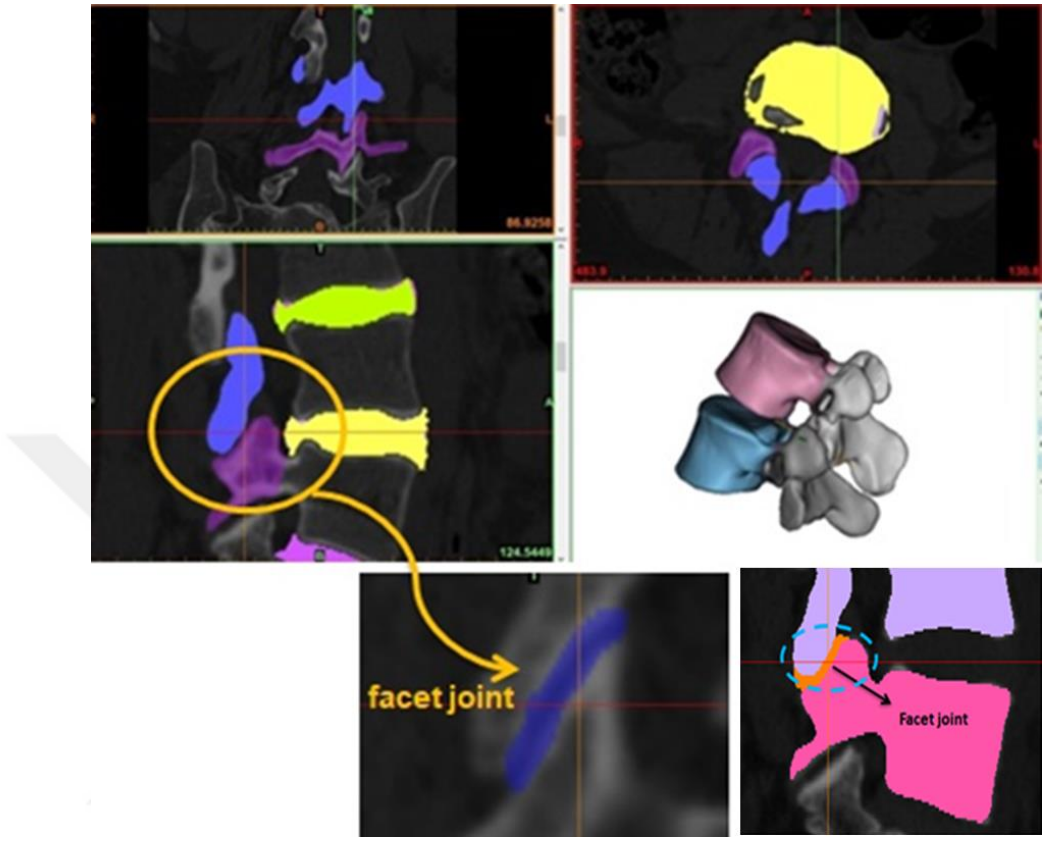

Figure 2.13: Manual segmentation of spinal components (intervertebral discs, facet joints, and vertebrae) with their views in different planes.

A certain thickness can be given to the facet cartilage elements in order not to allow any contact with the facet surfaces. Additionally, spring elements can also be used to represent the facet joint capsules in the models [54]. Another type of element that can be used for the construction of facet joints is interface gap elements to contact the facet surface areas [15], [41], [42]. Besides, facet joints can also be employed as shell elements in the modeling process [43]. Moreover, to mimic the contact between facet surfaces, the interface of the facet surfaces can be considered as a closed gap or opened gap by connecting or separating the nodes of these certain areas [55]. The facet joints have two distinct surfaces that have convex and concave sides [15], [29]. Du et al. used hex elements with a thickness of 0.1 mm to represent the facet cartilage surfaces in their study [56].

In finite element modeling, the surfaces between facet joint areas have been considered frictionless during the simulation processes [7], [24], [50], [56], [57]. Gong et al. used 0.6 mm mesh elements to define the facet cartilages in the modeling process. Besides, they used a friction coefficient of 0.1 to represent surface-to-surface contact element in their studies [6].

Facet joints can transmit the forces applied to the adjacent vertebrae of the spinal column [7], [49]. In order to define the sliding movement between vertebrae, although using the same meshing element type and same friction coefficient as Gong et al.[6], other researchers used 3D contact pairs for the construction of facet joints [7], [49].

2.3.3. Modeling of the ligaments

In the modeling process of spinal components, the construction of ligaments is also an important step to accurately define their regions in the spinal models. There are seven ligaments in the spine. These are anterior (ALL) and posterior longitudinal (PLL) ligaments, supraspinous (SSL) and interspinous (ISL)ligaments, intertransverse ligament (ITL), facet capsular ligament (FCL), and ligamentum flavum (LF) [2], [18], [58]. These ligaments can be represented by two-node 3D truss elements [10], 3D non-linear elements [58], and 10-node link elements [12], or with cord elements [4] in the modeling process. Additionally, linear and homogeneous type of tension-only spring elements can be employed for these structures [6]. Moreover, in several finite element studies, discrete spring elements, which had contact node behavior onto the adjacent vertebrae, were used for the modeling of ligaments. These structures were connected to the nodes of all the vertebral bones along the spinal column [54], [56].

To correctly define the anatomical structures of ligaments, a research group studied the biomechanical properties of human spinal ligaments [58]. They obtained cross-sectional area and length measurements from the living subjects and also from the fresh cadavers [58]. **Table 2.2** represented these measurements of all the ligaments of the spine. Manual segmentation of all the ligaments can be performed in medical imaging software with the help of this important information. **Figure 2.14** show the process of obtaining ligaments (anterior, posterior, and interspinous ligaments, and ligamentum flavum) by manual segmentation in different planes, and also represents the 3D model of these ligaments with the corresponding vertebrae.

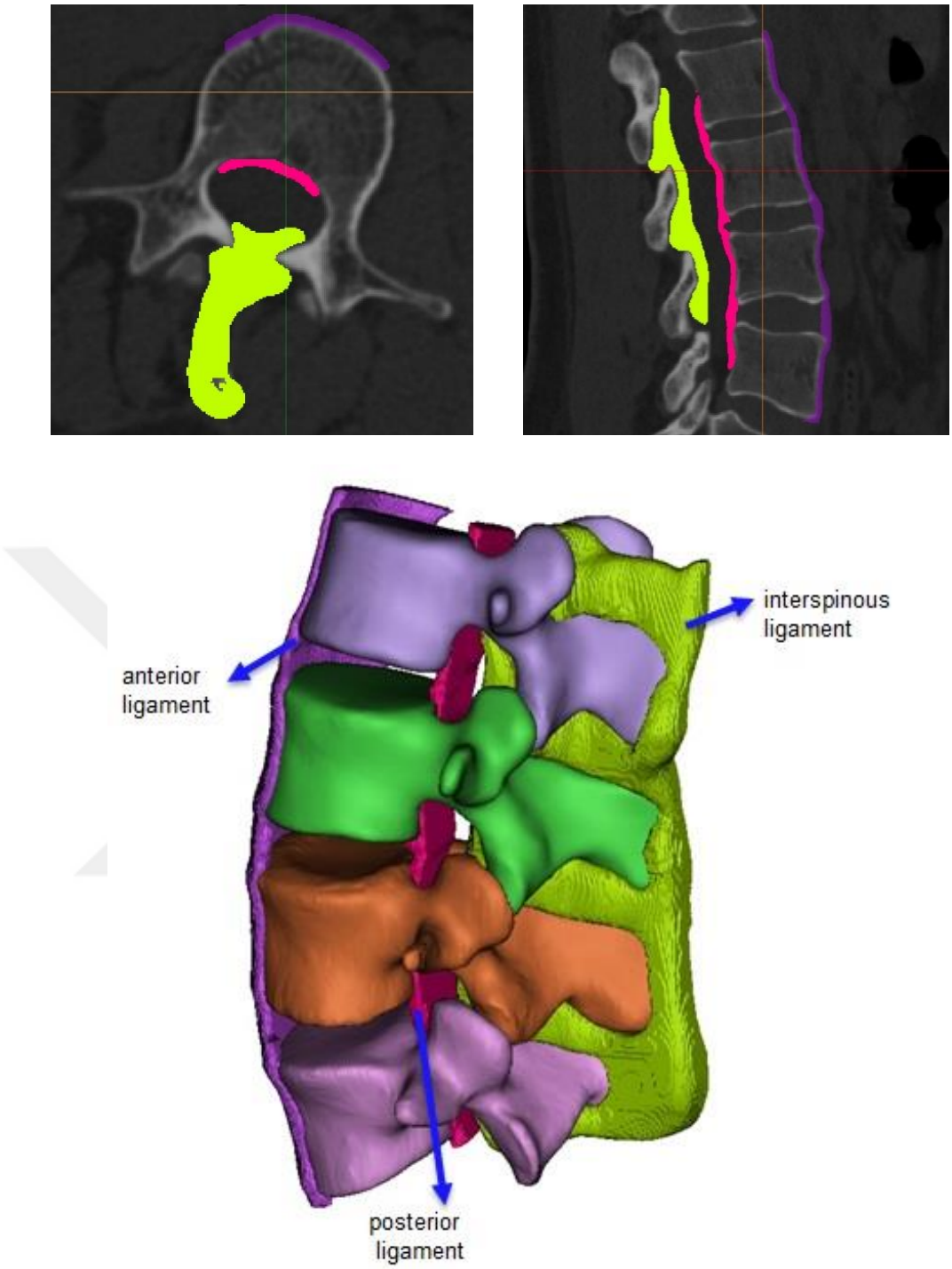

Figure 2.14: The 3D models of the ligaments after the segmentation process. Anterior, posterior, and interspinous ligaments of the L2-L5 model are seen [22].

Table 2.2: Cross-sectional area and length measurements of all the ligaments in the spine [58].

	Level	Cross-sectional area (mm^2)	Length (mm)
Anterior longitudinal ligament	C3-C4	13	6
	T4-T5	36	5
	T6-T7	30	6
	T10-T11	25	7
	L1-L2	44	11
	L3-L4	70	13
	L3-L4	74	12.5
	L4-L5	74	12.5
	L4-L5	66	12.5
Posterior longitudinal ligament	C2-C3	10	4.5
	C7-T1	11	5
	C7-T1	9	6
	T4-T5	17	6
	T12-L1	19	9.5
	L1-L2	20	11.5
	L2-L3	34	12.5
	L2-L3	26	10.5
	L2-L3	21	10.5
	L3-L4	19	12.5
Ligamentum flavum	T4-T5	34	12.5
	T5-T6	26	11.5
	T6-T7	29	13
	T7-T8	25	13

	T8-T9	19	13
	T10-T11	30	12
	L3-L4	39	19
Supra and interspinal ligament	T1-T2	9	12
	T2-T3	8	10.5
	T4-T5	8	10
	T7-T8	30	11
	T8-T9	29	10
	L3-L4	29	8
	L3-L4	34	12
	L4-L5	47	11.5
	L4-L5	55	9
	L4-L5	36	10
	L4-L5	24	12
	L4-L5	11	13
	L5-S1	26	11.5
	L5-S1	11	14
Intertransverse ligaments	T7-T8	1.7	8.5
	T9-10	2	9

2.3.4. Modeling of the spinal implants

The spinal instruments have been employed to correct the deformities of the spinal column. The improvements in spinal instrumentation in terms of their mechanical characteristics have been investigated by different research groups [6], [10]–[12], [44], [59], [60].

There are many different types of spinal implants used for the treatment of various spinal diseases. Posterior fusion surgeries have been performed with an intervertebral cage, pedicle screws, and rods [60]. Since screws and rods increase the fusion process of the

vertebral column, they have been used in spinal surgeries [44]. Material properties of the pedicles and rods can be stainless steel or titanium [44].

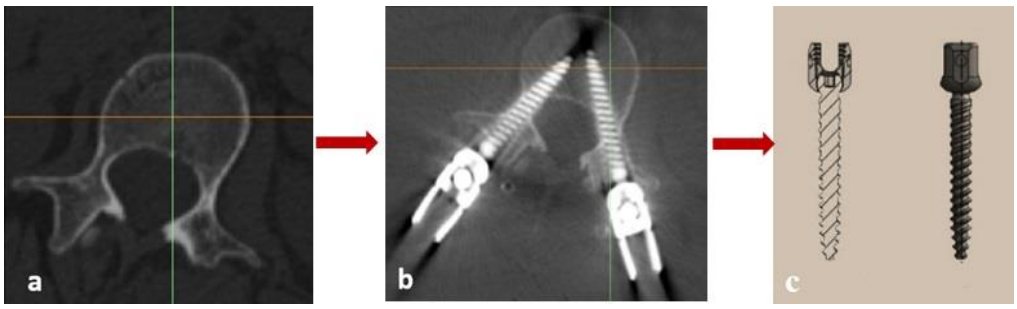

Figure 2.15: (a) The CT image of a vertebra before and (b) after the spinal fusion with pedicle screws. (c) The front and back of the screw structure used in spinal surgeries [22].

The spinal implants can be both made from metal sections such as titanium [6], [10], [12], [43], [44], titanium alloy [5], [12], [61] or stainless steel [44], and also they can be made from materials with elastic properties such as deformable rods with polymers [12] or PEEK materials [43], [44]. Dynamic spinal implantation systems can also be used in biomechanical studies [62]. The insertion process of pedicle screws into the lumbar vertebral body is represented in **Figure 2.15**.

CHAPTER 3

3. EXPERIMENTAL PART

The human spine involves hard tissues such as vertebral bodies and soft tissues like seven types of ligaments, intervertebral discs, and facet joints. The structure of vertebrae is also composed of two layers as cortical and trabecular regions. Additionally, the anatomical structure of the intervertebral disc is sub-sectioned with annulus and nucleus sections [63]. The functional spinal unit in biomechanical studies is known as the spine model with two vertebrae and the intervertebral disc that is located between them [15]. In this study, von Mises stress values were calculated for the L2-L3 and L2-L5 lumbar spine models with and without the implant systems.

In order to have a validated 3D model of the spine, there should be correct factors including mesh size, material properties, and geometric accuracy. In this study, CT scan data of an adolescent idiopathic patient was employed for the reconstruction process of the relevant spinal components. This data was obtained from a CT scanner (Siemens/Somatom Definition AS) with a slice thickness of 1.5 mm. Following the construction of all the important spinal components, detailed finite element spine models were obtained.

3.1. Construction of The L2-L3 Lumbar Spine Model

The functional spine unit of the L2-L3 lumbar spine model was developed from two-dimensional (2D) stacked CT scan images. The conversion of this data into 3D objects was completed by employing a medical image processing software (Mimics, Materialise's Interactive Medical Image Control System, Belgium). **Figure 3.1** indicates the reconstruction process of L2-L3 in different planes including coronal, sagittal, and axial regions.

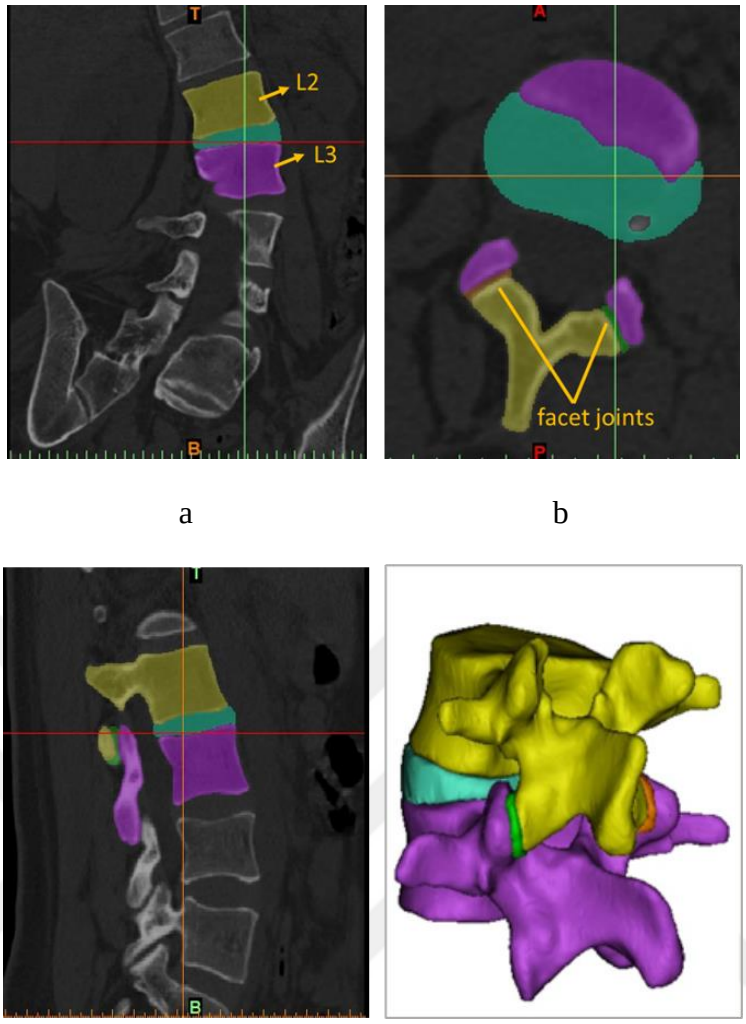

Figure 3.1: The segmentation process of L2-L3 lumbar vertebrae, the intervertebral disc between them, and the corresponding facet joints in coronal (a), axial (b), and sagittal (c) planes, and the 3D view of the whole model (d) [64].

L2-L3 model and its corresponding spinal components were constructed with several computer programs including Mimics and 3-Matic software (Mimics, Materialise's Interactive Medical Image Control System, Belgium) for the modeling sections and also Ansys workbench software (ANSYS 16.0, Ansys Inc. Canonsburg, PA, USA) for both constructions and also for the finite element analysis. The two-motion segment was reconstructed using the preset threshold values which were between 226-3071 HU for vertebral bones, in the medical imaging software. A series of manual editing operations were applied to the whole model components except the ligaments during the modeling process. These operations include cropping the mask to restrict the segmentation to a specified area, morphology, and multi-slice operations.

At the final stage, the two vertebrae, two facet joints, and an intervertebral disc between them were obtained with different segmentation masks. The completed model was obtained and smoothed without altering the features of the structures (**Figure 3.1, d**). After this construction step in the medical imaging software, all the spinal components were saved as stp (or step) (standard for the exchange of product model data) files for further processes.

After obtaining the 3D models, in the second stage of the construction of lumbar vertebrae, the bony structures were imported into another software, 3-Matic software (Mimics, Materialise's Interactive Medical Image Control System, Belgium), to apply the offset values of 1 mm to define the trabecular and cortical bone sections of the vertebrae [65].

After this stage, the stp files of vertebral bodies with two sections were imported into Ansys workbench software (ANSYS 16.0, Ansys Inc. Canonsburg, PA, USA) for finite element analysis. But before the simulation process, in a submodule of the software, Design Modeler, the trabecular and cortical regions of each lumbar vertebra were chosen and saved as a new part of this two-segmented model. The final version of the L2-L3 model involved these vertebral shells in the whole model. **Figure 3.2** shows the representation of the inner and outer shells of the lumbar vertebrae.

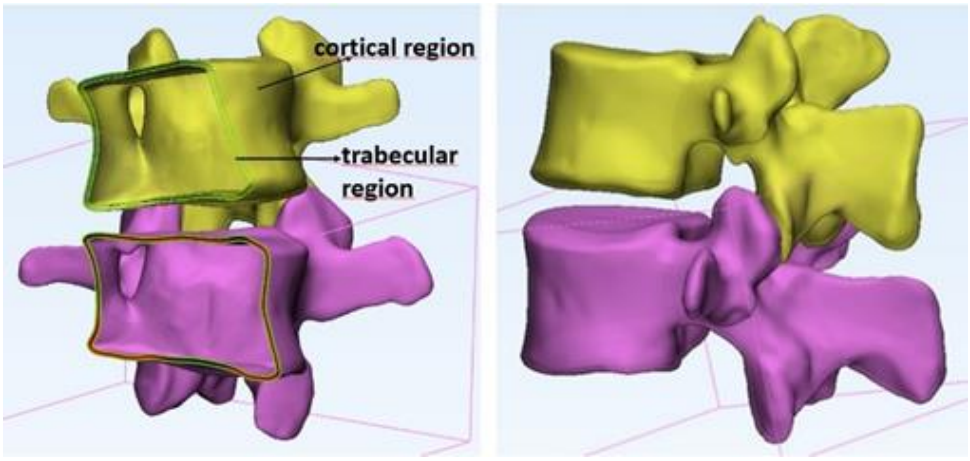

a b

Figure 3.2: The depiction of L2-L3 lumbar vertebrae with a) trabecular (the inner shell section) and the cortical (the outer shell section) parts, and b) the whole 3D model of the lumbar vertebrae [64].

In the Design Modeler of Ansys software, also the intervertebral disc was edited by separating the disc into annulus fibrosus and nucleus pulposus regions (**Figure 3.3**). The disc structure was also saved as a new part with the inner sections in the whole model.

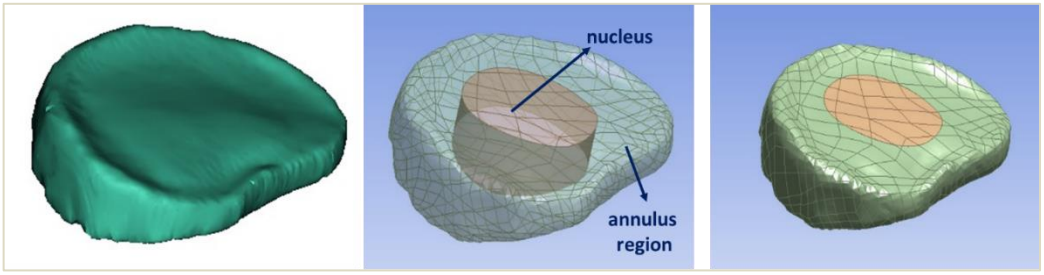

a b c

Figure 3.3: The construction of the L2-L3 intervertebral disc that was obtained from a) the segmentation process. The disc structure was separated as nucleus pulposus and annulus fibrosus in Ansys workbench software (b, c) [64].

3.1.1. Construction of the ligaments

Linear single force components were employed to define all the ligaments (anterior and posterior longitudinal, interspinous, supraspinous, ligamentum flavum, and intertransverse ligaments) of the L2-L3 lumbar spine model. Since the slack length of these ligaments was determined in the standing posture of the human body, a tensile force is obtained from these structures in the stretching position of the whole body [58], [66]. In this study, the relevant spinal ligaments of the lumbar spinal models were all determined as spring units [58], [66]. **Table 3.1** shows the stiffness values of ligaments that were obtained from in-vitro studies of human cadavers.

Table 3.1: The stiffness values of the ligaments from the literature that were based on experimental studies of the human spine [66], [67].

Ligament	**L2-L3 Model**
ALL	20.8 ± 14.0
PLL	36.6 ± 15.2
ISL	9.6 ± 4.8
SSL	24.8 ± 14.5
LF	25.1 ± 10.9
ITL	50.0

3.1.2. Construction of the spinal implant system

The spinal implant of this study involved rods and screws. The development of the pedicle screws was completed in Mimics software. In the 'analyze' section of this software, the cylindrical shapes were employed to construct these structures. Four pedicle screws were inserted bilaterally into the model. **Figure 3.4** indicates the screw trajectories in L2 and L3 lumbar vertebrae. All of the pedicles were constrained at the screw-bone interface. Manual adjustments of the length (60 mm) and the radius (2.5 mm) of the pedicles were determined.

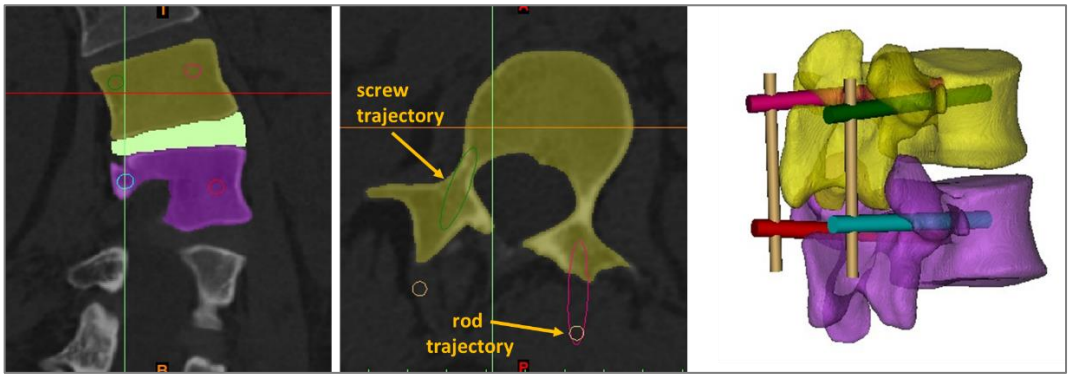

Figure 3.4: The description of the screw and rod trajectories in the L2-L3 lumbar spine model. The insertion of the pedicle screws in a) coronal and b) axial plane regions [64].

Additionally, there were two rods with a length of 55 mm and a radius of 1.8 mm attached to these pedicel screws. The rod trajectory is also given in **Figure 3.4**. The construction procedure of the rods was the same as the pedicle screws in Mimics software. In this study, both rods and screws were assigned as titanium-based materials.

3.1.3. Assignment of material properties of the spinal components

Before the simulation in Ansys workbench software, all the spinal components in the L2-L3 model, and also the fixed implant parts (rods and screws) were defined with their material properties including their modulus of elasticity and Poisson's ratio values. **Table 3.2** shows the materials that were assigned in the material library section of the software to each component of the model.

Table 3.2: Element types and material properties of the spinal components used in biomechanical studies.

Modeled spinal tissues and components of implants	Young's modulus (MPa)	Poisson's ratio	Element type	Reference
Cancellous bone	100	0.2	10-node tetrahedral element	[68]–[70]
Cortical bone	12000	0.3	10-node tetrahedral element	[63], [68]–[70]
Nucleus pulposus	1	0.499	10-node tetrahedral element	[63], [68], [70]
Annulus ground	8	0.49	10-node tetrahedral element	[65]
Pedicle screws and rods	110000	0.3	10-node tetrahedral element	[68], [70]

3.1.4. Meshing process of the L2-L3 model

The meshing procedure of all the L2-L3 lumbar spine models with and without the fixed implant system was performed with the help of Ansys workbench software (Ansys Workbench 16.0). The number of nodes was 494907 and the number of elements was 331453 for the intact model (without the implant system) (**Figure 3.5**). The other model with the fixed implant system had 154679 elements and 238562 nodes in the finite element model (**Figure 3.6**).

All the spinal components meshed with 10-node tetrahedral elements. The elements and material properties of the spinal structures are given in **Table 3.2**.

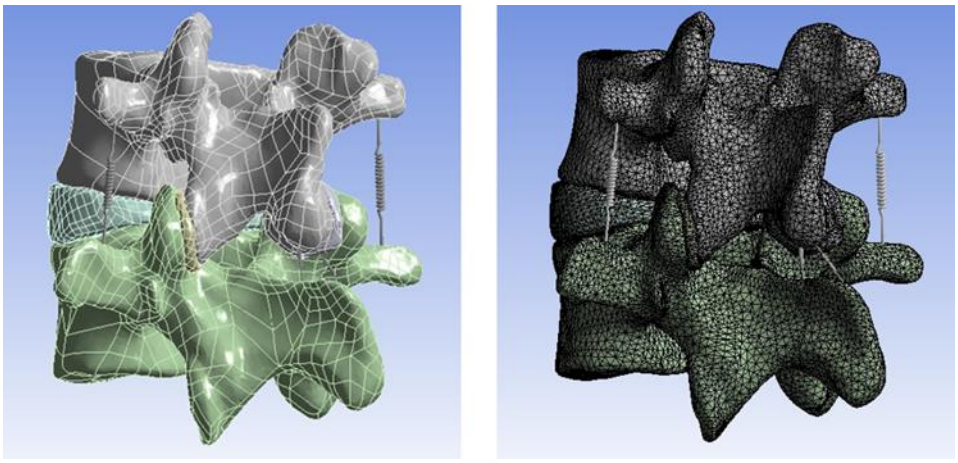

a b

Figure 3.5: The L2-L3 lumbar spine model without the implant system (the intact model) [64].

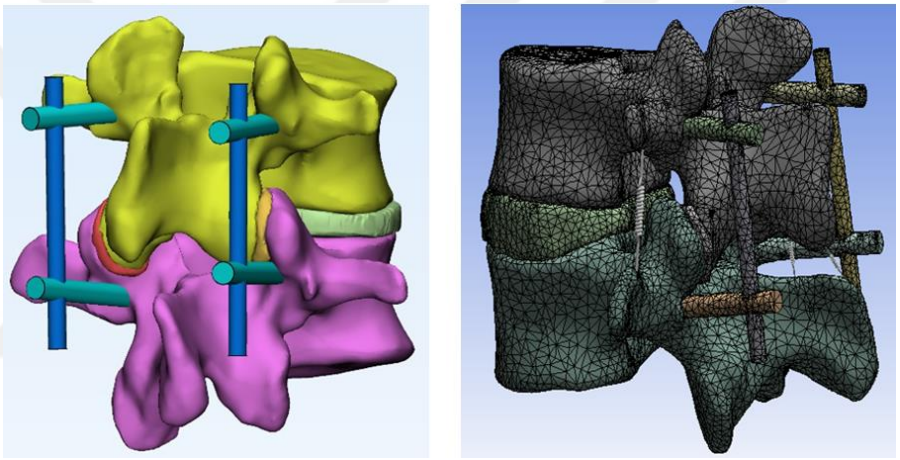

a b

Figure 3.6: The L2-L3 lumbar spine model with the pedicle screw implant system [64].

3.1.5. Boundary and loading conditions of the L2-L3 model

The boundary and loading conditions were applied to all of the L2-L3 models (with and without the implant system) for each movement including extension, lateral bending, flexion, and axial rotation. A pure moment with a combination of compression force was applied to the system. The local muscle forces and the body weight were represented by the applied compression force, and applying a pure moment is used to mimic the directional movements of the body.

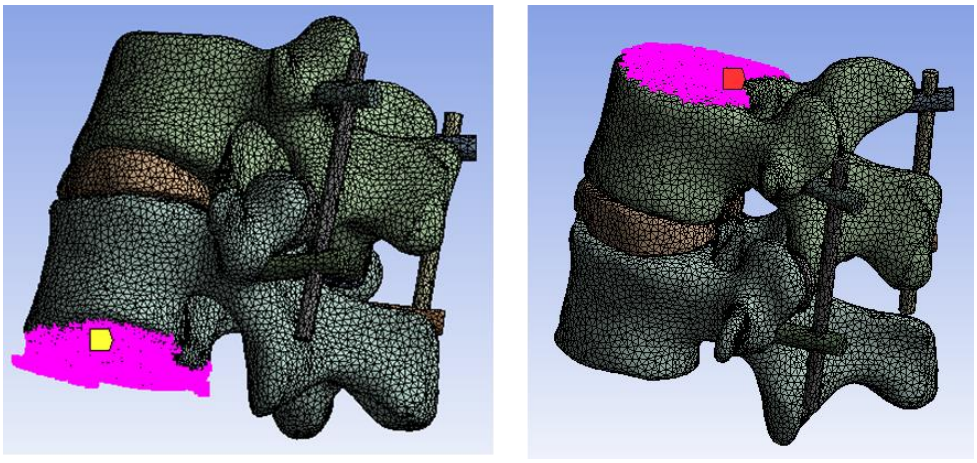

a b

Figure 3.7: The a) boundary (bottom surface of L3 vertebra) and b) loading conditions (top surface of L2 vertebra) of the L2-L3 lumbar spine model with the pedicle screw implant system [64].

As a boundary condition, the lower surface of the L3 vertebra was fixed and the compression forces were applied to the top of the L2 vertebra in the L2-L3 model (with and without the implant system) (**Figure 3.7**). These two-motion segment models were employed to measure the range of motion (ROM) values in four directional motions including flexion, extension, lateral bending, and axial rotation in the finite element analysis.

3.2. Construction of The L2-L5 Lumbar Spine Model

Similarly, the L2-L5 lumbar spine model was also developed with the same approach as the L2-L3 model. The same CT images from a patient suffering from adolescent idiopathic scoliosis were used in the modeling of the L2-L5 model. The reconstruction of 3D spinal components was obtained with the same medical imaging software. The constructed model with the fixed implant system is given in **Figure 3.7**.

In the reconstruction process, four lumbar vertebrae (L2-L5), three intervertebral discs (L2-L3, L3-L4, and L4-L5), six facet joints, and the corresponding ligaments (ligamentum flavum, interspinous ligaments, anterior and posterior longitudinal ligaments) were obtained with the same medical imaging software (Mimics Materialise's) as was used for the previous lumbar model. Also, the construction of the screw-rod system followed the same strategy. In the L2-L5 model, six pedicle screws with their trajectories in the second (L2), third (L3), and fifth (L5) vertebrae were completed. Again the

adjustments of all the screws and rods were manually performed in the software (**Figure 3.8**).

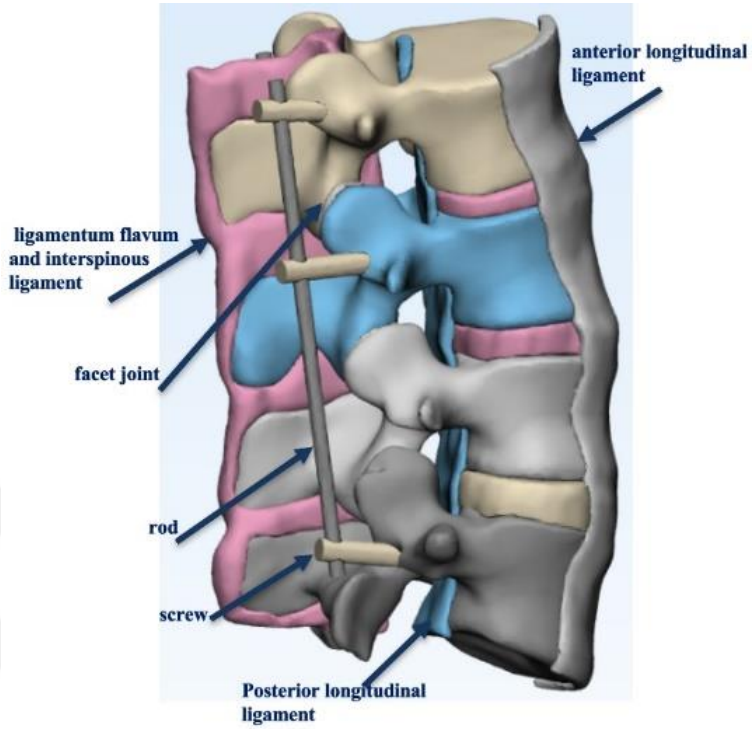

Figure 3.8: The L2-L5 lumbar spine model with the pedicle screw implant system [71]–[73].

The radius of each screw was 2.8 mm with a length of 48 mm in the model. The mechanical properties of the spinal components assigned to the L2-L5 model involved the same features as depicted in **Table 3.2**, except the intervertebral disc was kept as one part with an elastic modulus of 4.15 MPa, and a Poisson's ratio of 0.47. Moreover, PEEK material with an elastic modulus of 3600 MPa was used for the spinal rods in the construction of the model. Furthermore, the Ansys workbench was again used for the finite element analysis of the L2-L5 model.

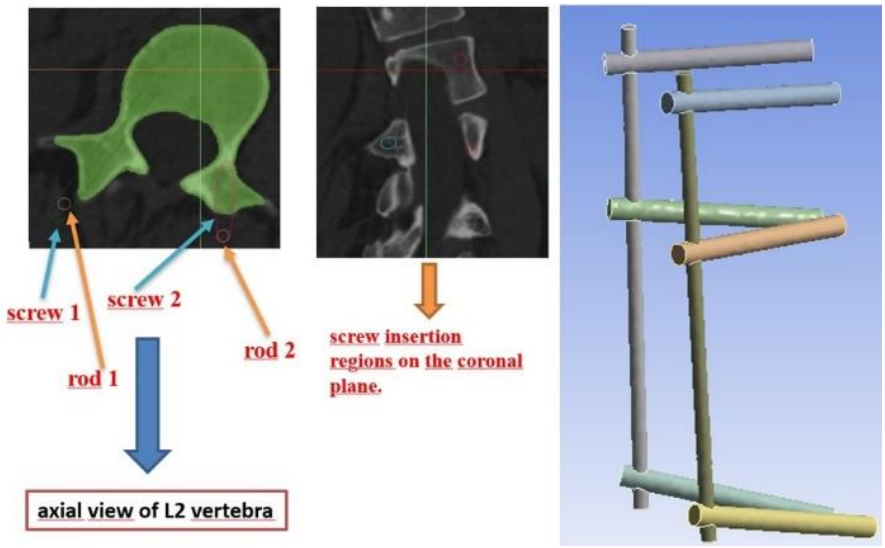

Figure 3.9: The development of the pedicle screw implant system [71]–[73].

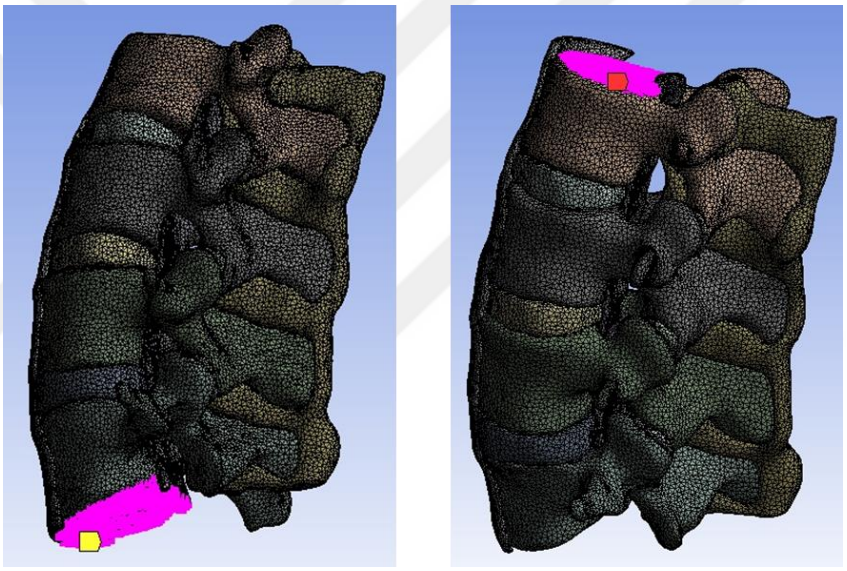

a b

Figure 3.10: The a) boundary (bottom surface of L5 vertebra) and b) loading conditions (top surface of L2 vertebra) of L2-L5 lumbar spine model with the pedicle screw implant system [71]–[73].

3.2.1. Meshing process of the L2-L5 model

The meshing of the L2-L5 lumbar model was performed by 3-Matic software with tetrahedral elements. The number of nodes of the intact model (the model without the implant system) was 234482, and the number of elements was 1261852. The meshed model of the implanted L2-L5 model was composed of 243363 nodes and 1296458 elements.

3.2.2. Boundary and loading conditions of the L2-L5 model

The boundary and loading conditions were also applied to the L2-L5 models (with and without the implant system) for each movement including extension, lateral bending, flexion, and axial rotation. Like the L2-L3 model, compression force and pure moment were applied to the spine model. As a boundary condition, the lower surface of the L5 vertebra was fixed and the compression forces were applied on the top of the L2 vertebra in the L2-L5 model (with and without the implant system) (**Figure 3.10**).

CHAPTER 4

4. RESULTS AND DISCUSSION

4.1. Validation Results for L2-L3 Lumbar Spine Model

In order to compare the ROM values of the models with and without the fixed implant system, experimental results were used from the literature [74].

For the model without any implantation system, ROM values for flexion were 2.7^{o}, for extension 2.4^{o}, for lateral bending 3.0^{o,} and 2.6^{o} for axial rotation. In this study, ROM values for the finite element model without any implantation system were in the range of the results of Lo et al. [74]. Besides, the ROM values for the lateral motion were also consistent with the in vivo results of this group [74].

In this study, the validation of the L2-L3 model with the fixed implant system was also investigated for flexion, extension, lateral bending, and axial rotation movements. The ROM values were measured as 2.3^{o} for flexion, 2.0^{o} for extension, 2.1^{o} for lateral bending, and 2.1^{o} for axial rotation. **Figure 4.1** represents ROM values of the assembly structures of the L2-L3 lumbar spine model with and without the fixed implant system.

The validation results were compared with the results of Lo et al. [74]. Similar ROM values were recorded for axial rotation and extension movements. Axial motion results were consistent with their study. Additionally, ROM values of the L2-L3 model with the fixed implant system for flexion and lateral bending were also in the range of the FE model of Lo et al. [74].

4.2. von-Mises Stress Distribution Results of L2-L3 Lumbar Spine Model

The equivalent von-Mises stresses were calculated for all the models with and without the spinal implant system. The stress distribution results over the intervertebral discs were represented in **Figure 4.2** and **Figure 4.3** including for all movement directions. The

color-changing indicates the intensity of the mechanical stress in the finite element analysis.

The maximum stress of the L2-L3 intervertebral disc was recorded as $1.67x10^6$ MPa (**Figure 4.2a**), and the stress result of the extension movement had a similar value (**Figure 4.2b**). But in lateral bending and axial rotation movements, the L2-L3 disc showed lower stress values. The stress value for lateral bending was recorded as $1.47x10^6$ MPa and it was decreased to $1.28x10^6$ MPa for axial rotation movement.

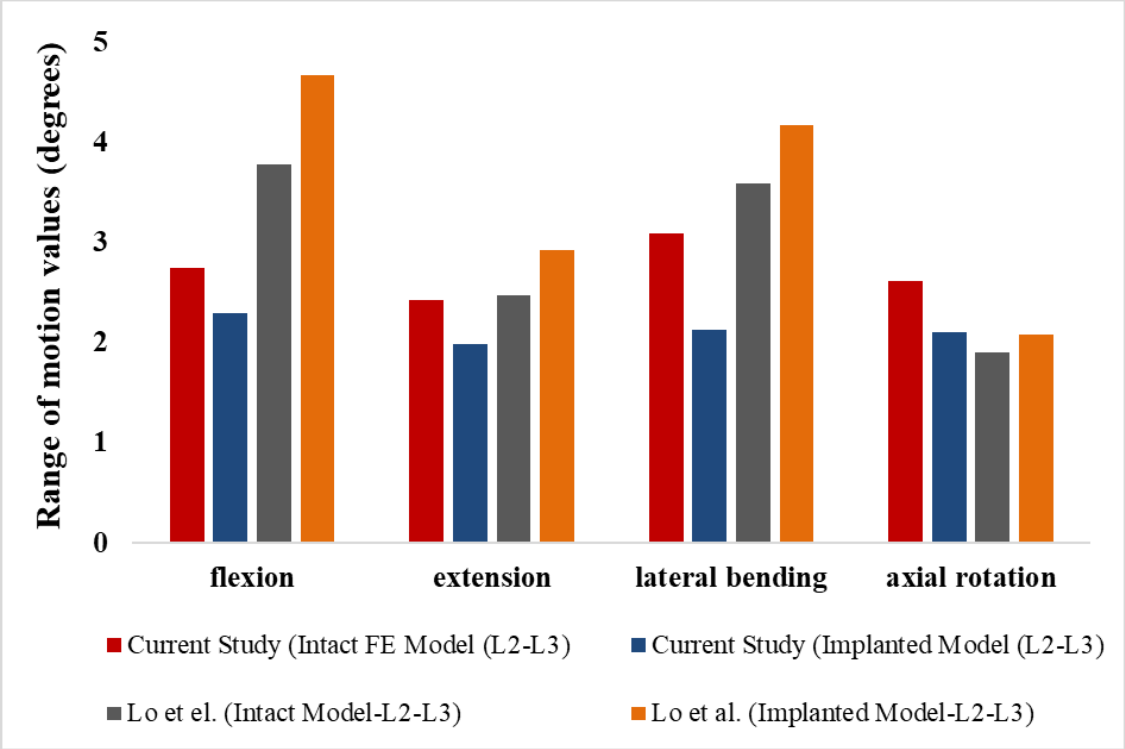

Figure 4.1: The ROM values of the L2-L3 lumbar spine model with and without the fixed implant system [75].

The intervertebral disc with the implanted model was also affected by the applied compression forces. However, the stress values of the L2-L3 model with the fixed implant system indicated lower stress values on the disc area (**Figure 4.3**). In flexion, the maximum stress was found as 1.32 MPa (**Figure 4.3a**). The stress values were close to each other in extension (0.86 MPa) (**Figure 4.3b**) and axial rotation (0.88 MPa) (**Figure 4.3c**) movements. For lateral motion, the von Mises stress result on the intervertebral disc was recorded as 1.04 MPa (**Figure 4.3d**) for the model with the fixed implant system.

Figure 4.4 represents the affected regions of the L2-L3 model without the implant system. With the color changing of the models, it was recorded that the intensity was much higher in the lateral motion. Besides, in lateral bending and flexion motion, the upper side of the

L2 vertebra expressed stress under the loading conditions. Moreover, the pedicle areas of the vertebral bodies indicated high von Mises stress distribution in extension, lateral bending, and axial rotation movements.

Additionally, the same simulations were performed for the model with the fixed implant system (**Figure 4.5**). According to these results, pedicle screws displayed stress values under the loading and boundary conditions of the model.

4.3. Discussion About The Results of The L2-L3 Lumbar Spine Model

In this study, the finite element model of the lumbar spine was constructed with all the spinal components. The CT data was obtained from a patient who was suffering from adolescent idiopathic scoliosis. The biomechanical behavior of a fixed spinal implant system (titanium screws and rods) was investigated in terms of the stress distribution affected on the intervertebral disc, lumbar vertebrae, and also on the screws and rods of the spinal implant system.

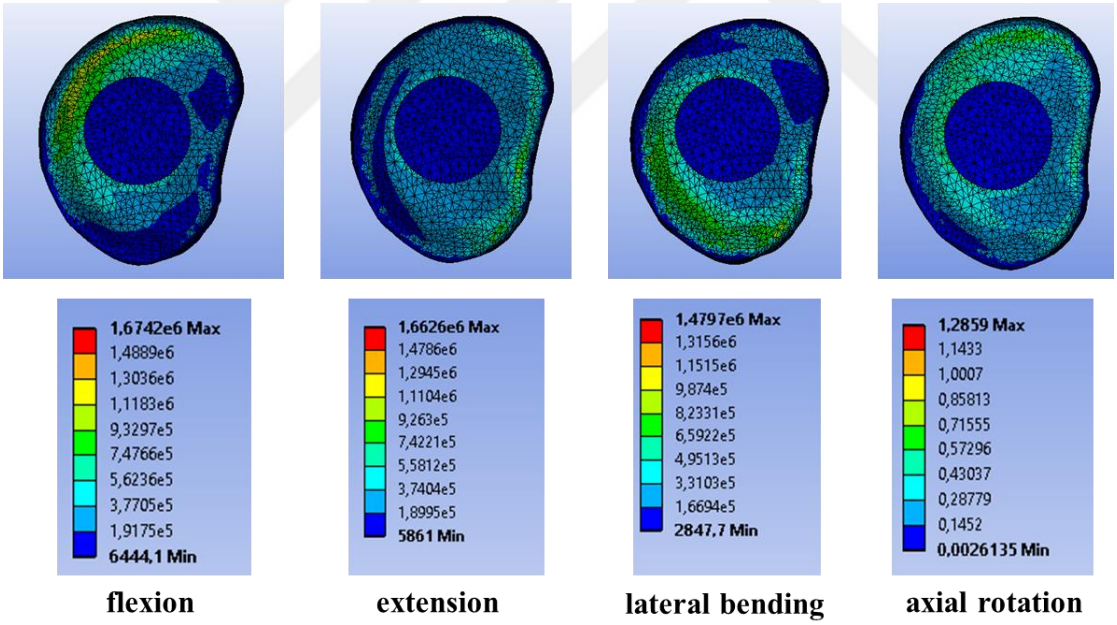

Figure 4.2: The representation of the von Mises stress analysis of the L2-L3 intervertebral disc without the fixed implant system. The stress distribution results were obtained for (a) flexion, (b) extension, (c) lateral bending, and (d) axial rotation [75].

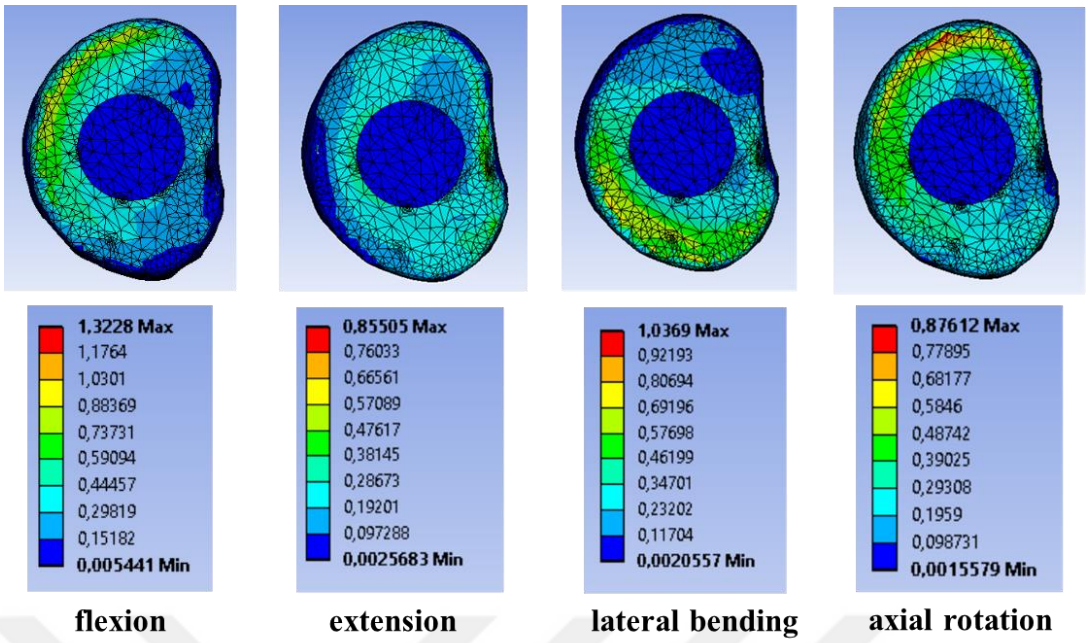

Figure 4.3: The representation of the von Mises stress analysis of the L2-L3 intervertebral disc with the fixed implant system. The stress distribution results were obtained for (a) flexion, (b) extension, (c) lateral bending, and (d) axial rotation [75].

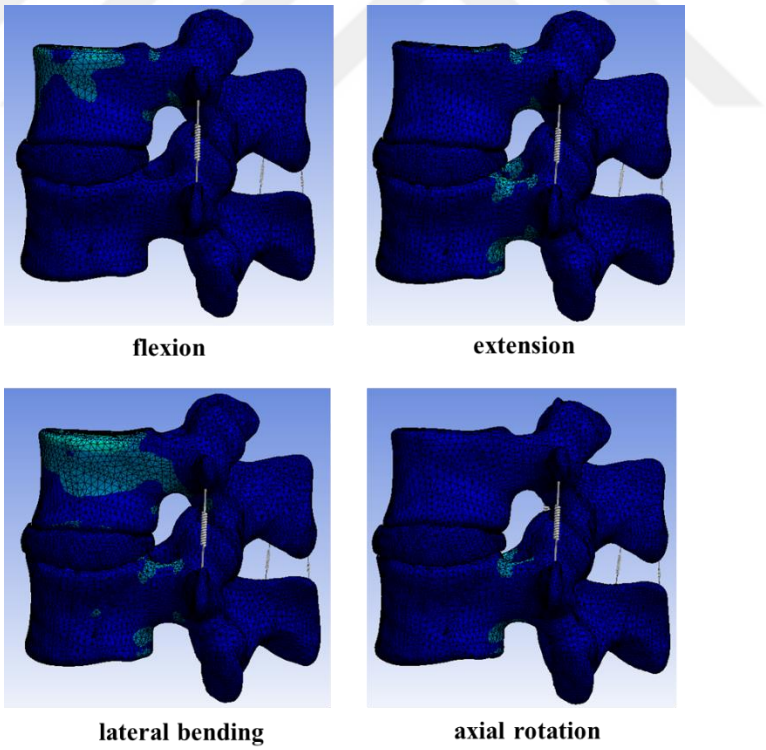

Figure 4.4: The representation of the stress analysis of the L2-L3 lumbar spine model without the fixed implant system. The stress distribution results were obtained for (a) flexion, (b) extension, (c) lateral bending, and (d) axial rotation under loading and boundary conditions [75].

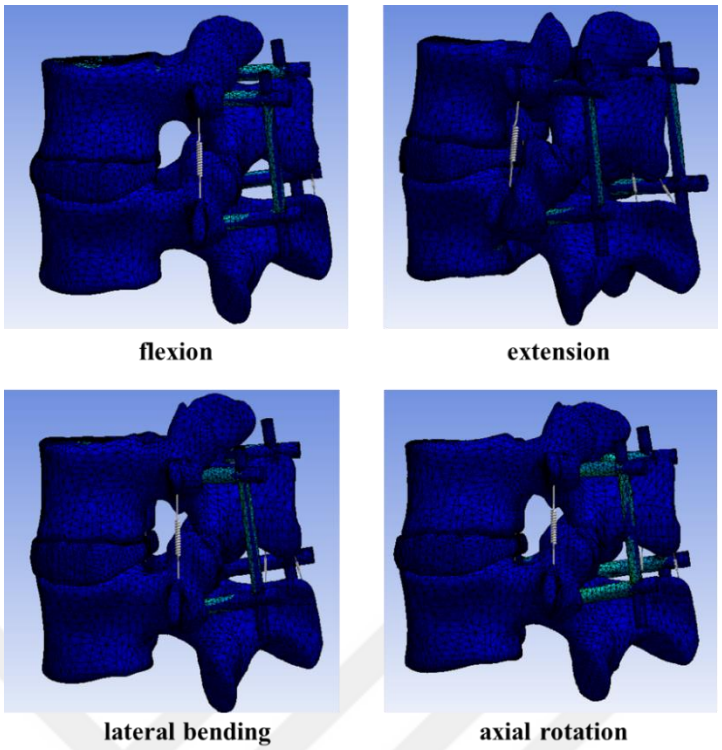

(a)

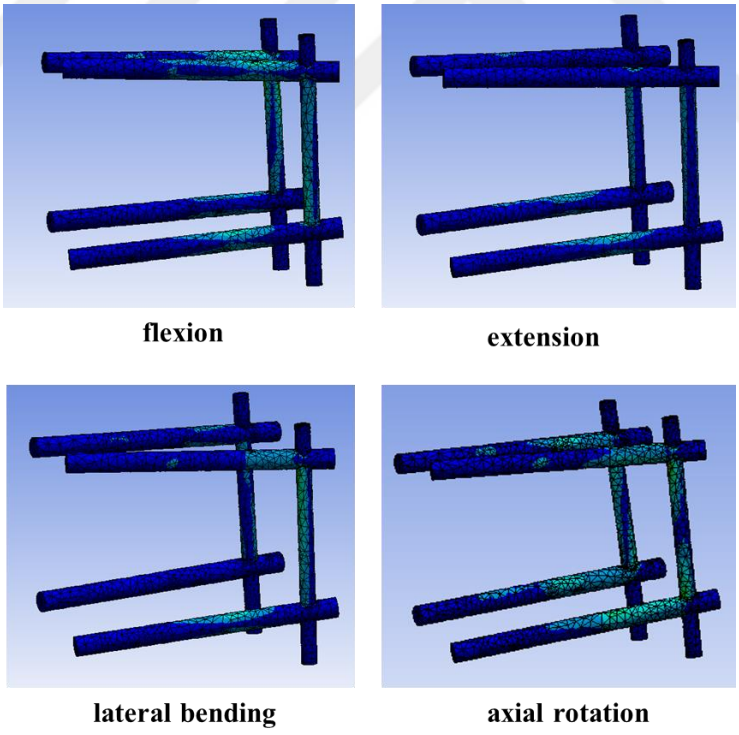

(b)

Figure 4.5: The representation of the stress analysis of the L2-L3 lumbar spine model with the fixed implant system. The stress distribution results were obtained for (a) flexion, (b) extension, (c) lateral bending, and (d) axial rotation under loading and boundary conditions. The stress distribution on the pedicle screws was recorded for each movement direction [75].

The loading conditions of the models, in four-movement directions including flexion, extension, lateral bending, and axial rotation, involved pure compression and moments both for the model with and without the implant system.

The ROM values that were depicted in **Figure 4.1** were the validation results of the L2-L3 lumbar spine model with and without the spinal implant. The comparison of the results was performed with the experimental data in the literature. According to these reported results by Lo et al. [74], the ROM values were found to be generally consistent with the data given in **Figure 4.1**. The ROM values of extension and axial rotation were in the range of this experimentally reported data of this group. Additionally, for flexion and lateral bending motions of the model, although there are slight differences between the ROM values, they were similar to the reported values as well (**Figure 4.1**).

The stress results showed that the top side of the L2 vertebra of the model without the implant system was the most affected part, especially in flexion and lateral bending (**Figure 4.4**). The maximum affected regions under loading conditions in extension and axial rotation motions were generally the pedicle regions of the vertebral bodies (**Figure 4.4**).

In this study, the loading conditions that were applied to the L2-L3 models with and without the implant system were 500 N compressive force and 8 Nm moment. These loading conditions were transmitted through the pedicle screws and rods in the finite element analysis. The results of this study showed that the screw-rod pedicle screw implant system decreased the stress distribution in the whole model. As depicted in **Figure 4.5**, the highest von Mises stress values were recorded at the rods in four directions of the lumbar model, but especially in flexion, axial rotation, and lateral bending motions (**Figure 4.5**).

According to the von-Mises stress analysis, in extension, flexion and lateral bending the model with the fixed spinal implant had maximum stress values on the rods. In extension motion, stress distribution displayed the lowest values when compared with the other directional movements (**Figure 4.5**). When compared with the intact model, the existence of the titanium implants decreased the stress distribution results in the L2-L3 model (**Figure 4.5**).

According to these results, the titanium implant allowed the system to stiffer. The stress values of the model without the implant system were lower than the intact model.

Moreover, the total deformation and von-Mises stress values were decreased on the L2-L3 intervertebral disc of the model with the fixed implantation. In addition to this, the finite element analysis results indicated that the maximum stress distribution was recorded at the interfaces of pedicle screws and rods in four directional movements including extension, flexion, lateral bending, and axial rotation.

In addition to this, the L2-L3 lumbar model was stabilized with these spinal instruments. Thus, all of the spinal components of the model with the fixed implant system indicated lower von-Mises stress distribution after achieving this stability. Lower stress values were specially recorded on the intervertebral disc of the model. Additionally, it was concluded that the most affected regions of the model were the pedicle screws and the rods of the spinal fixation system. Therefore, the intact model displayed higher stress distribution, especially on the pedicles of the vertebral bodies of the model.

4.4. von-Mises Stress Distribution Results of L2-L5 Lumbar Spine Model

The von-Mises stress results of the L2-L5 model indicated that the PEEK-based implant system decreased the stress and shear values if the results were compared with the traditional titanium fixed implant system. Also, the load sharing was recorded in terms of total deformation (**Figure 4.6**). The model without the implant system (the intact model), the model with the titanium-based implant system, and the model with the PEEK-based spinal implantation were compared.

The maximum equivalent stress for the intact model was recorded as 81.87 MPa, and maximum shear stress was also calculated as 45.57 MPa. The titanium-based screw-rod system had a higher maximum von-Mises stress distribution of 241.24 MPa, and maximum shear stress was recorded again higher than the intact model at 137.75 MPa.

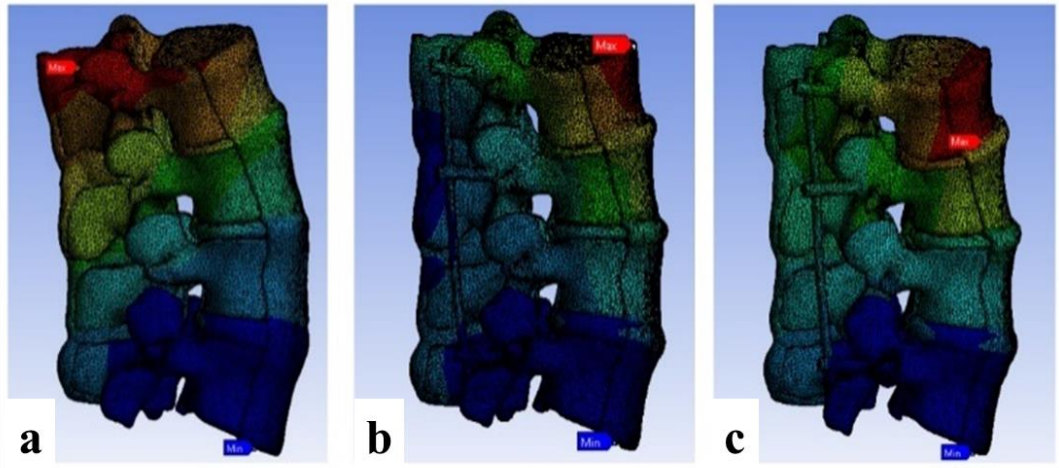

Figure 4.6: The representation of the total deformation results of the L2-L5 model with and without the fixation implant system. (a) intact model without the spinal fixation system, (b) the model with the titanium-rod system, and (c) the model with the PEEK-rod fixation implant system [71]–[73].

The PEEK-based spinal implant system had 115.17 MPa stress distribution and lower shear stress values of 58.84 for this study. It was noted that the bending of the model under the influence of loading conditions was greater in the titanium-based implant system. The PEEK-based system decreased the total deformation values by 15%, and also von Mises stress distribution was reduced by 53% in the L2-L5 lumbar spine model.

It was concluded that total deformation, von Mises stress distribution, and also the shear stress values were decreased with the existence of PEEK-based spinal instrumentation in this model. According to these results, it was noted that since the PEEK rod allowed the system to endure high stress as well as more balanced load sharing, the possibility of the adjacent segment disease was much higher in the model with the titanium-based fixed implantation system. PEEK-based implant decreased the stress distribution, especially on the interfaces of bone and screws.

4.5. Discussion About The Results of The L2-L5 Lumbar Spine Model

According to the finite element analysis results, the L2-L5 model with the PEEK-rod fixation system reduced the von Mises stress values, and also, the maximum affected regions were decreased under the loading conditions in the simulation (**Figure 4.6c**). The color-changing map of the model at the end of the analysis indicated that the affected areas were reduced in the PEEK-based system. The model without the implant system (intact model) was compared with the implanted models. In terms of total deformation results, there was not a significant difference between the PEEK-based and the titanium-

based implanted models. Therefore, the results of the finite element analysis indicated that the existence of the fixation system reduced the stress values applied on the models. It was concluded that the PEEK-based fixation system.

CHAPTER 5

5. CONCLUSIONS AND FUTURE WORK

In this study, two finite element lumbar models (L2-L3) were constructed with and without the spinal implants, and the biomechanical effect of the fixed spinal implant was investigated in terms of the von Mises stress distribution. According to these results, the existence of a fixed spinal implant system allowed to transmit of the applied forces through the screws and rods of the model in each directional movement including flexion, extension, lateral bending, and axial rotation. It was recorded that the model with the titanium implant system of the L2-L3 model had lower stress distribution results. Thus, this result indicated that the fixed implantation system allowed to stabilize the L2-L3 model.

The fixed implantation decreased mobility and preserved the maintenance of the whole lumbar model. Besides, this effect decreased the stress values on the adjacent intervertebral discs. Therefore, a fixed spinal implant can enhance the spinal injuries of the patients and can protect the adjacent segments from external damage. Furthermore, according to the results, it was pointed out that in the presence of fixation systems, both for the L2-L3 and also the L2-L5 lumbar spine models, the loading effect decreased on the spinal components, especially on the adjacent intervertebral discs.

In conclusion to the material properties of the fixation systems, the PEEK rod system can be considered a remarkable option for spinal fusion surgeries.

There are several limitations in this study. The first limitation was the absence of collagen fibers in the intervertebral discs. After obtaining the lumbar spine models, isotropic and elastic material properties were assigned to the nucleus pulposus before the simulation.

If there were collagen fibers in the annulus region of the discs and the hyper elastic materials were employed for the material properties, then the simulation process could have been enhanced.

Additionally, the construction process of the spine models of one patient is another limitation. The modeling and simulation stages of this study involve patient-specific characteristics. Moreover, the lack of muscle tissues in the constructed models was the other limitation of this study. The development of these tissues could not be modeled from CT scan data of the patient.

In future studies, different modeling methods of the spinal components and also the effect of different mechanical properties of the spinal implants will be investigated. Furthermore, the interfacing of musculoskeletal and finite element models will be performed with open-source software (Opensim) in order to conduct biomechanical modeling and simulation as well as dynamic simulations of the motor controls of the spinal models.

BIBLIOGRAPHY

[1] N. Boos and M. Aebi, *Spinal Disorders*. Springer, 2008.

[2] M. M. Panjabi and A. A. White, *Clinical Biomechanics of Spine*, 2nd ed. J.B.Lippincott Company, 1990.

[3] J. A. Janicki and B. Alman, "Scoliosis: Review of diagnosis and treatment.," *Paediatr Child Health*, vol. 12, no. 9, pp. 771–776, 2007, doi: 10.1067/mmt.2002.123336.

[4] J. Zheng, Y. Yang, S. Lou, D. Zhang, and S. Liao, "Construction and validation of a three-dimensional finite element model of degenerative scoliosis," *Journal of Orthopaedic Surgery and Research*, vol. 10, no. 1, pp. 1–7, 2015, doi: 10.1186/s13018-015-0334-1.

[5] J. P. Little, M. T. Izatt, R. D. Labrom, G. N. Askin, and C. J. Adam, "An FE investigation simulating intra-operative corrective forces applied to correct scoliosis deformity," *Scoliosis*, vol. 8, no. 9, pp. 1–13, 2013, doi: 10.1186/1748-7161-8-9.

[6] Z. Gong, Z. Chen, Z. Feng, Y. Cao, C. Jiang, and X. Jiang, "Finite element analysis of 3 posterior fixation techniques in the lumbar spine," *Orthopedics*, vol. 37, no. 5, pp. 441–448, 2014, doi: 10.3928/01477447-20140430-54.

[7] F. Xie, H. Zhou, W. Zhao, and L. Huang, "A comparative study on the mechanical behavior of intervertebral disc using hyperelastic finite element model," *Technology and Health Care*, vol. 25, no. S1, pp. 177–187, 2017, doi: 10.3233/THC-171320.

[8] W. Wang, G. R. Baran, R. R. Betz, A. F. Samdani, J. M. Pahys, and P. J. Cahill, "The Use of finite element models to assist understanding and treatment for scoliosis: A review paper," *Spine Deformity*, vol. 2, no. 1, pp. 10–27, 2014, doi: 10.1016/j.jspd.2013.09.007.

[9] J. Clin, C. É. Aubin, N. Lalonde, S. Parent, and H. Labelle, "A new method to include the gravitational forces in a finite element model of the scoliotic spine," *Medical and Biological Engineering and Computing*, vol. 49, no. 8, pp. 967–977, 2011, doi: 10.1007/s11517-011-0793-4.

[10] Y. Abe, M. Ito, K. Abumi, H. Sudo, R. Salmingo, and S. Tadano, “Scoliosis corrective force estimation from the implanted rod deformation using 3D-FEM analysis,” *Scoliosis*, vol. 10, no. Suppl 1, p. S2, 2015, doi: 10.1186/1748-7161-10-S2-S2.

[11] A. Shirazi-Adl, M. El-Rich, D. G. Pop, and M. Parnianpour, “Spinal muscle forces, internal loads and stability in standing under various postures and loads - Application of kinematics-based algorithm,” *European Spine Journal*, vol. 14, no. 4, pp. 381–392, 2005, doi: 10.1007/s00586-004-0779-0.

[12] S. Zahaf and S. Kebdani, “Biomechanical Study between the Rigid and Dynamic Fixation Systems of the Spinal Column Analyzed by the Finite Element Method,” *Nano Biomedicine & Engineering*, vol. 9, no. 2, pp. 169–183, 2017, doi: 10.5101/nbe.v9i2.p169-183.

[13] F. M. Saavedra-Pozo, R. A. M. Deusdara, and E. C. Benzel, “Adjacent segment disease perspective and review of the literature,” *Ochsner Journal*, vol. 14, no. 1, pp. 78–83, 2014.

[14] S. Moaveni, *Finite element analysis—theory and application with ANSYS*, vol. 12, no. 8. Upper Saddle River, New Jersey: Prentice-Hall, 1999. doi: 10.1016/s0892-6875(99)90030-4.

[15] M. A. Tyndyk, V. Barron, P. E. McHugh, and D. O’Mahoney, “Generation of a finite element model of the thoracolumbar spine,” *Acta of Bioengineering and Biomechanics*, vol. 9, no. 1, pp. 35–46, 2007, [Online]. Available: http://ovidsp.ovid.com/ovidweb.cgi?T=JS&PAGE=reference&D=emed8&NEWS=N&AN=2008045577

[16] M. J. Fagan, S. Julian, and A. M. Mohsen, “Finite element analysis in spine research,” *Proceedings of the Institution of Mechanical Engineers, Part H: Journal of Engineering in Medicine*, vol. 216, no. 5, pp. 281–298, 2002, doi: 10.1243/09544110260216568.

[17] G. Chen *et al.*, “A new approach for assigning bone material properties from CT images into finite element models,” *Journal of Biomechanics*, vol. 43, no. 5, pp. 1011–1015, 2010, doi: 10.1016/j.jbiomech.2009.10.040.

[18] S. M. Kurtz and A. A. Edidin, *Spine Technology Handbook*. Elsevier Academic Press, 2006.

[19] C. VanPutte, J. Regan, and A. Russo, *Seeley's Essentials of Anatomy & Physiology*. Mc Graw Hill Education, 2016.

[20] I. Shojaei, B. D. Hendershot, J. C. Acasio, C. L. Dearth, M. Ballard, and B. Bazrgari, "Trunk muscle forces and spinal loads in persons with unilateral transfemoral amputation during sit-to-stand and stand-to-sit activities," *Clinical Biomechanics*, vol. 63, pp. 95–103, 2019, doi: 10.1016/j.clinbiomech.2019.02.021.

[21] R. Subach, B., M. Martin, M., C. Copay, A., B. Califanp, C., B. Claasses, L., and L. A. Bologna, "Spines in Motion:Biomechanics of the Spine," *Spinal Research Foundation*, vol. 7, no. 2, p. 64, 2012.

[22] S. Z. Akinci and Y. Z. Arslan, "Finite element spine models and spinal instruments: a review," *Journal of Mechanics in Medicine and Biology*, vol. 22, no. 04, p. 2230001, 2022, doi: 10.1142/S0219519422300010.

[23] H. Schmidt, F. Galbusera, A. Rohlmann, and A. Shirazi-Adl, "What have we learned from finite element model studies of lumbar intervertebral discs in the past four decades?," *Journal of Biomechanics*, vol. 46, no. 14, pp. 2342–2355, 2013, doi: 10.1016/j.jbiomech.2013.07.014.

[24] N. v. Jaumard, W. C. Welch, and B. A. Winkelstein, "Spinal facet joint biomechanics and mechanotransduction in normal, injury and degenerative conditions," *Journal of Biomechanical Engineering*, vol. 133, no. 7, pp. 1–31, 2011, doi: 10.1115/1.4004493.

[25] T. Hines, "Functional anatomy of the spine," *Mayfield Clinic Brain & Spine*, pp. 1–5, 2016, doi: 10.1016/B978-0-444-53486-6.00032-6.

[26] M. Rao, "Explicit Finite element modeling of the human lumbar spine," 2010. doi: 10.5772/281.

[27] C. Celenk and P. Celenk, *Bone Density Measurement Using Computed Tomography*. InTech, 2012.

[28] H. Huang, C. Xiang, C. Zeng, H. Ouyang, K. K. L. Wong, and W. Huang, "Patient-specific geometrical modeling of orthopedic structures with high efficiency and accuracy for finite element modeling and 3D printing," *Australasian Physical and*

Engineering Sciences in Medicine, vol. 38, no. 4, pp. 743–753, 2015, doi: 10.1007/s13246-015-0402-1.

[29] C. R. Hassan, "Finite Element Model Development of the Human Lumbar Spine and Dynamic Stabilization Device Analysis," Koc University, 2015.

[30] C. Chen *et al.*, "CT morphometric analysis to determine the anatomical basis for the use of transpedicular screws during reconstruction and fixations of anterior cervical vertebrae," *PLoS ONE*, vol. 8, no. 12, pp. 1–10, 2013, doi: 10.1371/journal.pone.0081159.

[31] W. R. Hotchkiss, R. M. Schwend, P. P. Bosch, H. J. H. Edgar, and B. N. Young, "Defining the Differences in Transverse Plane Trajectories for Thoracic Pedicle Screw Insertion: Anatomic Versus Medial," *Spine Deformity*, vol. 4, no. 1, pp. 22–26, 2016, doi: 10.1016/j.jspd.2015.05.004.

[32] X. Hu, K. B. Siemionow, and I. H. Lieberman, "Thoracic and lumbar vertebrae morphology in Lenke type 1 female adolescent idiopathic scoliosis patients.," *International Journal of Spine Surgery*, vol. 8, no. 30, pp. 1–12, 2014, doi: 10.14444/1030.

[33] J. U. Yoo, A. Ghanayem, C. Petersilge, and J. Lewin, "Accuracy of using computed tomography to identify pedicle screw placement in cadaveric human lumbar spine," *Spine*, vol. 22, no. 22. pp. 2668–2671, 1997. doi: 10.1097/00007632-199711150-00016.

[34] Y. H. Kim, B. Khuyagbaatar, and K. Kim, "Recent advances in finite element modeling of the human cervical spine," *Journal of Mechanical Science and Technology*, vol. 32, no. 1, pp. 1–10, 2018, doi: 10.1007/s12206-017-1201-2.

[35] D. Chen *et al.*, "Three-dimensional reconstructions in spine and screw trajectory simulation on 3D digital images: a step by step approach by using Mimics software," *Journal of Spine Surgery*, vol. 3, no. 4, pp. 650–656, 2017, doi: 10.21037/jss.2017.10.09.

[36] I. M. D. C. C. Silva, D. Q. de Freitas, G. M. B. Ambrosano, F. N. Bóscolo, and S. M. Almeida, "Bone density: Comparative evaluation of hounsfield units in multislice and cone-beam computed tomography," *Brazilian Oral Research*, vol. 26, no. 6, pp. 550–556, 2012, doi: 10.1590/S1806-83242012000600011.

[37] J. J. Schreiber, A. P. Hughes, F. Taher, and F. P. Girardi, “An Association Can Be Found Between Hounsfield Units and Success of Lumbar Spine Fusion,” *Hospital for Special Surgery Journal*, vol. 10, no. 1, pp. 25–29, 2014, doi: 10.1007/s11420-013-9367-3.

[38] Dogru, S. Cansel, Cansız, Erol, Arslan, and Yunus Ziya, “A Review of Finite Element Applications in Oral and Maxillofacial Biomechanics,” *Journal of Mechanics in Medicine and Biology*, no. vi, pp. 1–26, 2018, doi: 10.1142/S0219519418300028.

[39] Z. Yosibash, N. Trabelsi, and C. Milgrom, “Reliable simulations of the human proximal femur by high-order finite element analysis validated by experimental observations,” *Journal of Biomechanics*, vol. 40, no. 16, pp. 3688–3699, 2007, doi: 10.1016/j.jbiomech.2007.06.017.

[40] C. S. Aparna, R. P. Tewari, and A. K. Govil, “Biomechanical Analysis of a Three Dimensional Finite Element Model,” *International Journal on Theoretical and Applied Research in Mechanical Engineering*, vol. 2, no. 2, pp. 155–158, 2013.

[41] I. Zafarparandeh, D. U. Erbulut, and A. F. Ozer, “Influence of three-dimensional reconstruction method for building a model of the cervical spine on its biomechanical responses: A finite element analysis study,” *Advances in Mechanical Engineering*, vol. 8, no. 3, pp. 1–6, 2016, doi: 10.1177/1687814016638809.

[42] F. Ezquerro, A. Simón, M. Prado, and A. Pérez, “Combination of finite element modeling and optimization for the study of lumbar spine biomechanics considering the 3D thorax-pelvis orientation,” *Medical Engineering and Physics*, vol. 26, no. 1, pp. 11–22, 2004, doi: 10.1016/S1350-4533(03)00128-0.

[43] Q. B. Lv *et al.*, “Biomechanical properties of novel transpedicular transdiscal screw fixation with interbody arthrodesis technique in lumbar spine: A finite element study,” *Journal of Orthopaedic Translation*, vol. 10, no. 15, pp. 50–58, 2018, doi: 10.1016/j.jot.2018.08.005.

[44] F. Galbusera, C. M. Bellini, F. Anasetti, C. Ciavarro, A. Lovi, and M. Brayda-Bruno, “Rigid and flexible spinal stabilization devices: A biomechanical comparison,” *Medical Engineering and Physics*, vol. 33, no. 4, pp. 490–496, 2011, doi: 10.1016/j.medengphy.2010.11.018.

[45] H. E. Jaramillo, L. Gómez, and J. J. García, “A finite element model of the L4-L5-S1 human spine segment including the heterogeneity and anisotropy of the discs,” *Acta of Bioengineering and Biomechanics*, vol. 17, no. 2, pp. 15–24, 2015, doi: 10.5277/ABB-00046-2014-02.

[46] N. Momeni Shahraki, A. Fatemi, V. K. Goel, and A. Agarwal, “On the Use of Biaxial Properties in Modeling Annulus as a Holzapfel-Gasser-Ogden Material,” *Frontiers in Bioengineering and Biotechnology*, vol. 3, no. 69, pp. 1–9, 2015, doi: 10.3389/fbioe.2015.00069.

[47] H. Farajpour and N. Jamshidi, “Effects of different angles of the traction table on lumbar spine ligaments: A finite element study,” *Clinics in Orthopedic Surgery*, vol. 9, no. 4, pp. 480–488, 2017, doi: 10.4055/cios.2017.9.4.480.

[48] D. J. Coombs, P. J. Laz, M. Rao, S. D. Smith, B. M., and P. J. Rullkoetter, “Stepwise Validated Finite Element Model of the Human Lumbar Spine,” in *SIMULIA Customer Conference*, 2012, pp. 1–15.

[49] V. Palepu, “Biomechanical Effects of Initial Occupant Seated Posture During Rear End Impact Injury,” The University of Toledo, 2013.

[50] L. Wang, B. Zhang, S. Chen, X. Lu, Z. Y. Li, and Q. Guo, “A Validated Finite Element Analysis of Facet Joint Stress in Degenerative Lumbar Scoliosis,” *World Neurosurgery*, vol. 95, pp. 126–133, 2016, doi: 10.1016/j.wneu.2016.07.106.

[51] S. P. Faria, “Biomechanical Analysis of the Human Lumbar Spine An Experimental and Computational Approach,” no. May 2015, 2015.

[52] K. S. Emanuel, A. J. van der Veen, C. M. E. Rustenburg, T. H. Smit, and I. Kingma, “Osmosis and viscoelasticity both contribute to time-dependent behaviour of the intervertebral disc under compressive load: A caprine in vitro study,” *Journal of Biomechanics*, vol. 70, pp. 10–15, 2018, doi: 10.1016/j.jbiomech.2017.10.010.

[53] H. M. Raheem, B. Bay, and S. Rochefort, “Viscoelastic properties of a novel hydrogel/foam composites for nucleus pulposus replacement,” *Springer Nature Applied Sciences*, vol. 1, no. 809, pp. 1–9, 2019, doi: 10.1007/s42452-019-0855-z.

[54] T. L. Bredbenner, T. D. Eliason, W. L. Francis, J. M. McFarland, A. C. Merkle, and D. P. Nicolella, “Development and Validation of a Statistical Shape Modeling-

Based Finite Element Model of the Cervical Spine Under Low-Level Multiple Direction Loading Conditions," *Frontiers in Bioengineering and Biotechnology*, vol. 2, no. 58, pp. 1–12, 2014, doi: 10.3389/fbioe.2014.00058.

[55] R. Krueger, J. G. Ratcliffe, and P. J. Minguet, "Panel stiffener debonding analysis using a shell/3D modeling technique," *Composites Science and Technology*, vol. 69, no. 14, pp. 2352–2362, 2009, doi: 10.1016/j.compscitech.2008.12.015.

[56] C.-F. Du, N. Yang, J.-C. Guo, Y.-P. Huang, and C. Zhang, "Biomechanical response of lumbar facet joints under follower preload: a finite element study," *BMC Musculoskeletal Disorders*, vol. 17, no. 126, pp. 1–13, 2016, doi: 10.1186/s12891-016-0980-4.

[57] J. Q. Campbell and A. J. Petrella, "An automated method for landmark identification and finite-element modeling of the lumbar spine," *IEEE Transactions on Biomedical Engineering*, vol. 62, no. 11, pp. 2709–2716, 2015, doi: 10.1109/TBME.2015.2444811.

[58] J. Chazal *et al.*, "Biomechanical properties of spinal ligaments and a histological study of the supraspinal ligament in traction," *Journal of Biomechanics*, vol. 18, no. 3, pp. 167–176, 1985, doi: 10.1016/0021-9290(85)90202-7.

[59] H. C. Chen *et al.*, "Biomechanical evaluation of a novel pedicle screw-based interspinous spacer: A finite element analysis," *Medical Engineering and Physics*, vol. 46, pp. 27–32, 2017, doi: 10.1016/j.medengphy.2017.05.004.

[60] C. Herren *et al.*, "Biomechanical testing of a PEEK-based dynamic instrumentation device in a lumbar spine model," *Clinical Biomechanics*, vol. 44, pp. 67–74, 2017, doi: 10.1016/j.clinbiomech.2017.03.009.

[61] C. Kim, S. M. Son, S. H. Choi, T. S. Goh, J. S. Lee, and C. Lee, "Numerical Evaluation of Spinal Stability after Posterior Spinal Fusion with Various Fixation Segments and Screw Types in Patients with Osteoporotic Thoracolumbar Burst Fracture Using Finite Element Analysis," *Applied Sciences*, vol. 11, pp. 1–18, 2021.

[62] C. Chen, C. Huang, and S. Shih, "Biomechanical evaluation of a new pedicle screw-based posterior dynamic stabilization device (Awesome Rod System) - A

finite element analysis," *BMC Musculoskeletal Disorders*, vol. 16, no. 81, pp. 1–8, 2015, doi: 10.1186/s12891-015-0538-x.

[63] N. Salsabili, J. Santiago López, and M. I. Prieto Barrio, "Simplifying the human lumbar spine (L3/L4) material in order to create an elemental structure for the future modeling," *Australasian Physical and Engineering Sciences in Medicine*, vol. 42, no. 3, pp. 689–700, 2019, doi: 10.1007/s13246-019-00768-z.

[64] S. Z. Akinci, H. K. Surmen, D. Karabulut, S. C. Dogru, O. Yaman, and Y. Z. Arslan, "Biomechanical Effect of an Implant System on Lumbar Spinal Segments," in *Xth International Biomechanics Congress*, 2021, p. SS-28, 50.

[65] Y. Fan, S. Zhou, T. Xie, Z. Yu, X. Han, and L. Zhu, "Topping-off surgery vs posterior lumbar interbody fusion for degenerative lumbar disease: A finite element analysis," *Journal of Orthopaedic Surgery and Research*, vol. 14, no. 1, pp. 1–15, 2019, doi: 10.1186/s13018-019-1503-4.

[66] M. Putzer, S. Auer, W. Malpica, F. Suess, and S. Dendorfer, "A numerical study to determine the effect of ligament stiffness on kinematics of the lumbar spine during flexion," *BMC Musculoskeletal Disorders*, vol. 17, no. 1, pp. 1–8, 2016, doi: 10.1186/s12891-016-0942-x.

[67] F. A. ; Pintar, N. ; Yoganandan, T. ; Myers, A. ; Elhagediab, and A. Sances Jr., "Biomechanical Properties of Human Lumbar Spine Ligaments," *Journal of Biomechanics*, vol. 25, no. 11, pp. 1351–1356, 1992, doi: doi:10.1016/0021-9290(92)90290-h.

[68] T. Lu and Y. Lu, "Interlaminar stabilization offers greater biomechanical advantage compared to interspinous stabilization after lumbar decompression: a finite element analysis," *Journal of Orthopaedic Surgery and Research*, vol. 15, no. 1, pp. 1–12, 2020, doi: 10.1186/s13018-020-01812-5.

[69] M. Song *et al.*, "Stress distribution of different lumbar posterior pedicle screw insertion techniques: a combination study of finite element analysis and biomechanical test," *Scientific Reports*, vol. 11, no. 1, pp. 1–15, 2021, doi: 10.1038/s41598-021-90686-6.

[70] C. Liu, A. Kamara, and Y. Yan, “Investigation into the biomechanics of lumbar spine micro-dynamic pedicle screw,” *BMC Musculoskeletal Disorders*, vol. 19, no. 1, pp. 1–11, 2018, doi: 10.1186/s12891-018-2132-5.

[71] S. Z. Akinci, D. Karabulut, H. K. Surmen, O. Yaman, and Y. Z. Arslan, “The Effect of PEEK-Rod Fixation Systems on Finite Element Lumbar Spine Model,” *European Journal of Science and Technology*, no. 34, pp. 783–786, 2022, doi: 10.31590/ejosat.1086952.

[72] S. Z. Akinci, D. Karabulut, H. K. Surmen, and O. Yaman, “The Effect of PEEK-Rod Fixation Systems on Finite Element Lumbar Spine Model,” in *2nd International Conference on Applied Engineering and Natural Sciences (ICAENS)*, 2022, p. 484.

[73] S. Z. Akinci, D. Karabulut, H. K. Surmen, O. Yaman, and Y. Z. Arslan, “The Investigation of The Effect of PEEK-Rod Fixation Systems on Pedicle Screws and The Adjacent Intervertebral Discs,” in *4th International Conference on Medical Devices (ICMD)*, 2021, p. 25.

[74] C. C. Lo, K. J. Tsai, S. H. Chen, Z. C. Zhong, and C. Hung, “Biomechanical effect after Coflex and Coflex rivet implantation for segmental instability at surgical and adjacent segments: A finite element analysis,” *Computer Methods in Biomechanics and Biomedical Engineering*, vol. 14, no. 11, pp. 969–978, 2011, doi: 10.1080/10255842.2010.502894.

[75] S. Z. Akinci, H. K. Surmen, D. Karabulut, O. Yaman, and Y. Z. Arslan, “Construction and Validation of Functional Lumbar Spine Unit,” in *2nd International Symposium of Scientific Research and Innovative Studies (ISSRIS’22), 02-05 March*, 2022, pp. 1349–1351.

MECHANICAL ANALYSIS OF SPINAL IMPLANTS IN PATIENTS WITH ADOLESCENT IDIOPATHIC SCOLIOSIS

ORIGINALITY REPORT

15%	12%	11%	3%
SIMILARITY INDEX	INTERNET SOURCES	PUBLICATIONS	STUDENT PAPERS

PRIMARY SOURCES

1	etd.uthsc.edu Internet Source	1%
2	www.ncbi.nlm.nih.gov Internet Source	1%
3	Submitted to Eastern Mediterranean University Student Paper	1%
4	www.researchsquare.com Internet Source	1%
5	Tianhao Wang, Zhihua Cai, Yongfei Zhao, Wei Wang, Guoquan Zheng, Zheng Wang, Yan Wang. "The Influence of Cross-Links on Long-Segment Instrumentation Following Spinal Osteotomy: A Finite Element Analysis", World Neurosurgery, 2019 Publication	<1%
6	link.springer.com Internet Source	<1%
7	mountainscholar.org	